Development of NIR luminescent N-acetyl-L-cysteine coated Ag_2S quantum dots with differential therapeutic effect

Pelin Turhan Buz[1], Fatma Demir Duman[1], Merve Erkisa[2], Gozde Demirci[3], Ferda Ari[4], Engin Ulukaya[*2] & Havva Yagci Acar[*1,5]

[1]Koc University, Department of Chemistry, Istanbul 34450, Turkey

[2]Istinye University, Department of Clinical Biochemistry, School of Medicine, Istanbul 34010, Turkey

[3]Koc University, Graduate School of Materials Science and Engineering, Rumelifeneri Yolu, Sariyer, Istanbul 34450, Turkey

[4]Uludag University, Department of Biology, Bursa 16059, Turkey

[5]Koc University, Surface Science and Technology Center (KUYTAM), Istanbul 34450, Turkey

* Authors for correspondence:

Havva Yagci Acar : E-mail: fyagci@ku.edu.tr; Phone: +90 (212) 338 1742

Engin Ulukaya : E-mail : eulukaya@istinye.edu.tr; Phone: +90 (0)850 283 69 10

First draft submitted: 22 June 2018; Accepted for publication: 3 January 2019; Published online: TBC

Aim: N-acetyl-l-cysteine (NAC) is a free radical scavenger. We developed NAC coated Ag_2S (NAC-Ag_2S) QDs as an optical imaging and therapeutic agent. **Materials & methods:** QDs were synthesized in water. Their optical imaging potential and toxicity were studied *in vitro*. **Results:** NAC-Ag_2S QDs produced with strong emission that is tunable between 748-840 nm, were stable in biologically relevant media. QDs showed significant differences both in cell internalization and toxicity *in vitro*. QDs were quite toxic to breast and cervical cancer cells but not to lung derived cells despite the higher uptake. NAC-Ag_2S reduces reactive oxygen species (ROS) but causes cell death via DNA damage and apoptosis. **Conclusion:** NAC-Ag_2S NIR QDs are stable and strong signal generating theranostic agents offering selective therapeutic effect.

Keywords: N-acetyl-l-cysteine (NAC), Ag_2S quantum dots, imaging, apoptosis, reactive oxygen species (ROS), DNA damage

Introduction

Luminescent semiconductor nanocrystals (quantum dots, QDs) have received great attention in the last two decades, especially in bioimaging, biolabeling, diagnosis and therapy, with their excellent properties such as size-tunable emission, higher resistance against photobleaching, broader excitation and narrower emission spectra compared to organic fluorophores, which are commonly used in biological applications [1-3]. Recently, there is a great effort towards development of QDs with strong luminescence in the near-infrared region (NIR), since autofluorescence and absorption by living tissues are strong in the visible region of the spectrum. Some cellular structures like collagen show

considerable autofluorescence and biological chromophores, in particular oxy- and deoxyhemoglobin cause luminescence quenching due to absorption and scattering of the light in the visible region [4]. Absorbance of water above 900 nm is also an important limitation. Hence, 700-900 nm region is accepted as the optical imaging window where the absorption coefficient of tissue is at its minimum and penetration depth of the light is higher [5, 6]. The most common NIRQDs which were tested for biolabeling, biosensing, *in vitro* and *in vivo* bioimaging applications are CdHgTe [7], CdHgTe/CdS [8], CdSeTe [9], and PbS [10]. Major road blocker for the transition of such QDs into the clinic is the potential health risks related to the presence of heavy metals in these compositions [11, 12].

Ag_2S QDs emerged as a new class of QDs with emission in the NIR region and became very popular with the highly biocompatible, stable and strongly luminescent nature [13-16]. Very low solubility constant (K_{sp} = 6.3 x 10^{-50}) inhibits the release of Ag^+ ions into the biological media and ensures high biocompatibility [17]. In determining the biocompatibility of QDs, the organic coating around the crystalline QD core is also important. It does not only influence the QD-cell interaction, biodistribution and biocompatibility, but also it controls the particle growth, provide colloidal stability and surface functionality for the conjugation of desired ligands, peptides, drugs or oligonucleotides to QDs for specific action [18-20]. Ag_2S QDs were synthesized with several functional coating materials in the literature such as 2-mercaptopropionic acid (2-MPA) [16], dimercaptosuccinic acid (DMSA) which is a heavy metal chelator [21], bovine serum albumin (BSA) [22], polyethylene glycol [14], ribonuclease-A (RNase A) [17] or with mixed coatings such as polyethyleneimine (PEI)/2-MPA [15] and

PEI/cysteine [23]. These studies demonstrate the impact of coating on particle size, emission wavelength and toxicity.

Use of biologically relevant molecules as a coating for QDs is a popular approach to render QDs less toxic. N-acetyl-l-cysteine (NAC), which is a derivative of cysteine, falls under this category. Emission tunable synthesis of NIR emitting CdTe/CdS capped with NAC via hydrodynamic route [24] and folic acid tagged-NAC/CdTeS for targeted *in vivo* tumor imaging [25] are couple of examples to successful use of NAC as a coating material on QDs. Besides, inhibition of beta 1-40 amyloid fibrillation, which is one of the primary factors inducing Alzheimer's disease, with NAC/CdTe QDs [26] and selective determination of 4c4 [27], copper [28] or Hg(II) [29] are some examples to different uses of NAC coated QDs from the literature.

NAC is a well-known antioxidant and a source of sulfhydryl group which is converted into metabolites in cells stimulating glutathione synthesis [30]. Hence, it is a natural scavenger of free radicals, especially reactive oxygen species (ROS), thereby it has been used as a pharmaceutical product in the diseases induced by free radicals [31-33]. NAC can be utilized to protect the tissues from the cytotoxicity of chemotherapeutic cancer drugs [34, 35]. NAC is also used to protect cells from oxidative stress and reduce QD-induced cytotoxicity [36-38].

ROS have an important role in regulatory pathways [39]. Singlet oxygen ($O^{\cdot}$), superoxide [$O_2^{\cdot-}$], hydroxyl radicals [$^{\cdot}OH$]), and peroxides (hydrogen peroxide [H_2O_2]) are the products of mitochondrial respiratory chain and are the constituents of ROS. In normal cells, ROS level is kept at a certain level while cancer cells have an abnormally high level of ROS [40]. QD based toxicity is, at least partially, attributed to ROS generation [36, 38]. Increasing ROS level is usually associated with cell death. However, downregulation of

ROS in apoptotic cancer cells was also reported for some antioxidants and NAC, as well [41, 42]. ROS scavenging effect of NAC was demonstrated in the literature [43-45]. However, bioavailability and stability of NAC is limited due the presence of reactive sulfhydryl group [43]. During the intravenous administration, NAC forms a disulfide bond with human serum albumin which limits its bioavailability [46]. One approach to improve its bioavailability is to render it more lipophilic and membrane permeable by forming its ethyl ester [47] or amide derivative [48]. These approaches slightly improved the bioavailability of NAC in plasma. Conjugation of NAC to polymeric or dendrimeric carriers via a disulfide bond, which will cleave *in vivo* and release NAC, was reported to reduce ROS level more than the free NAC, which suggests better bioavailability via reduction of NAC-serum protein interaction [43, 49].

In this study, we synthesized highly luminescent, stable and NIR emitting NAC coated aqueous Ag_2S QDs for the first time in the literature and evaluated the toxicity and imaging potential in several cell lines. Initially, variables such as the NAC amount, Ag/S ratio and reaction temperature was studied to produce the QDs with high colloidal stability and strong luminescence in biologically relevant media (pH 7.4 and pH 4.5 dH_2O, 10 mM NaCl, PBS and FBS). Later, cytotoxicity of NAC-Ag_2S on several cell lines (A549, BAES-2, HeLa and MCF-7) was determined. An unprecedented therapeutic potential of NAC-Ag_2S was discovered. Influence of NAC-Ag_2S QDs on ROS level, apoptosis and DNA-damage was examined on the most vulnerable MCF-7 cell line, in a dose and time dependent manner. Free NAC was also used for comparison. NAC-Ag_2S emerged as a stable, effective optical label and a selective therapeutic agent.

Materials & methods

Materials

Silver nitrate ($AgNO_3$, 99.9999%) and 2-(N-morpholino) ethanesulfonic acid (MES) were purchased from Aldrich (MO, USA). Sodium sulfide (Na_2S) was purchased from Alfa-Aesar (Lancashire, England). N-acetyl-l-cysteine (NAC), sodium hydroxide (NaOH), acetic acid (CH_3COOH), sodium chloride (NaCl), Suprapur nitric acid (65%) and Suprapur sulphuric acid (96%) were obtained from Merck Millipore (MA, USA). LDS 798 NIR laser dye was purchased from Exciton Inc. (OH, USA). Vivaspin 20 centrifugal filters (3000 Da MW cut-off) were obtained from Sartorius (Goettingen, Germany). Roswell Park Memorial Institute 1640 medium (RPMI 1640, 1x), trypsin EDTA and penicillin-streptomycin solutions were provided by Multicell, Wisent Inc. (QC, Canada). Fetal bovine serum (FBS) was obtained from Capricorn Scientifc GmbH (Ebsdorfergrund, Germany). Thiazolyl blue tetrazolium bromide (MTT) and phosphate-buffered saline (PBS) tablets were purchased from Biomatik Corp. (ON, Canada). Dimethyl sulfoxide Hybri-Max™ and 4′,6-diamidino-2-phenylindole (DAPI) were obtained from Sigma (MO, USA). 4% paraformaldehyde solution in PBS was purchased from Santa Cruz Biotechnology, Inc. (CA, USA). All 12-, 24- and 96-well plates were obtained from Nest Biotechnology Co. Ltd. (Wuxi, China). Only ultra-pure water (18.2 MΩ, Rephile Biosciences and Technology, Shanghai, China) was used when water is needed. All reagents were of analytical grade or of the highest purity.

Synthesis of N-acetyl-l-cysteine coated Ag_2S QDs

In a typical reaction, $AgNO_3$ (0.125 mmol) and N-acetyl-l-cysteine (NAC) (0.25 mmol) were dissolved in 37.5 ml of deionized (DI) water in a reaction flask and pH of the

solution was adjusted to 10 using NaOH and CH_3COOH solutions (1 M) under Ar flow. Na_2S (0.03125 mmol) was dissolved in 12.5 ml of DI water in a separate 25 ml round-bottom flask and sonicated under Ar flow for 30 minutes. Then, the Na_2S solution was injected to the reaction mixture at 70°C under vigorous mechanical stirring (Figure 1). In order to follow the particle growth, 3 mL aliquots were taken from the reaction solution at different time points. At the end, reaction mixture was cooled down to room temperature (RT) and QDs were washed with DI water using Vivaspin 20 centrifugal filters. Aqueous QDs are stored in the dark at 4°C.

Reaction variables such as Ag/S, Ag/NAC, reaction temperature and reaction time were studied to understand their influence on the optical properties and stability of QDs. Table 1 summarizes all recipes and the properties of the resulting QDs.

In addition, dried QDs were dissolved in different biologically relevant media (pH 7.4 and pH 4.5 dH_2O, 10 mM NaCl, PBS and FBS) for the determination of their stability and optical properties in these media.

Characterization Methods

All characterization methods are described in full detail in the associated Supplementary information document.

Cell Culture

Human bronchial epithelial cell line (BEAS-2B), human lung adenocarcinoma cell line (A549) and human cervical cancer cell line (HeLa) were cultured in RPMI 1640 medium supplemented with 10% FBS, 100 U/mL penicillin, 100 μg/mL streptomycin and 1% L-glutamine. Human breast cancer cell line (MCF-7) was cultured in RPMI 1640 medium

containing 5% fetal bovine serum, 100 U/mL penicillin, 100 μg/mL streptomycin and 1% L-glutamine. All these cell lines were incubated at 37°C under 5% CO_2 atmosphere in a humidified incubator.

ATP viability assay

The luminogenic ATP assay was used to determine the level of cellular ATP as an indirect measure of the number of viable cells. Cytotoxicity of NAC-Ag_2S QDs and free NAC at equivalent concentrations to NAC content of QDs (Supplementary Table 2) on MCF-7, A549, HeLa and BEAS-2B cells were determined by the ATP viability assay. All cells were seeded at a density of 5×10^3 cells per well with 100 μL of culture medium in 96-well plates and allowed for cell growth for 24 h in a 37°C under 5% CO_2 atmosphere in a humidified incubator.. Then, cells were treated with QDs or free NAC in various concentrations (0.10–200 μg/ml) and incubated under same conditions for another 24 h or 48 h. At the end of the incubation period, 50 μl of ATP-releasing reagent (a detergent-based reagent) was added to each well and incubated at room temperature for 20–30 min to extract the intracellular ATP from the cells. 50 μl of this suspension from each well and 50 μl luciferin–luciferase mixture per well (FLAAM, Sigma Aldrich, US) were transferred into a white opaque 96-well plate. Luminescence from each well was determined with a Bio-Tek Luminometer (USA). Viability of the treated cells was calculated with reference to the untreated controls. All experiments were performed in triplicate.

Intracellular Uptake of QDs

Intracellular uptake of NAC-Ag_2S QDs was quantitatively determined from the intracellular Ag concentrations measured by ICP-MS (inductively coupled plasma–mass

spectroscopy). All cell lines were seeded at a density of 1.75×10^5 cells/well in 6-well plates and incubated for 24 h at 37°C under 5% CO_2 humidified incubator. Then, cells were treated with NAC-Ag_2S QDs at 100 µg/mL nanoparticle concentration and incubated for 1h. Cell media of each well were collected in separate tubes and attached cells were washed with 2 mL of PBS (pH 7.4). PBS used for the washing step was combined with the removed media from the cells. Then, attached cells were detached using trypsin/EDTA, transferred into a centrifuge tube and precipitated at 1500 rpm. After being washed with 4 mL of PBS in order to remove un-internalized QDs, precipitated cells were transferred into 10 mL volumetric flasks with 2 mL deionized water. The cell precipitates in the flasks were dried on a hot plate and treated with 1 mL acid mixture (ultrapure H_2SO_4 and HNO_3 (1:9 v/v)) for at least 1 week. The cell lysates were diluted to 10 mL volume with deionized water and Ag ion concentration of the samples were measured by ICP-MS using a freshly prepared Ag standard curve. All experiments were repeated 4 times and data is reported as the average.

In order to evaluate the cellular uptake of QDs optically and demonstrate its imaging potential, QD treated cells were imaged under fluorescent microscope. All cell lines were seeded into 6-well plates at a density of 1.75 x 10^5 cells/well and incubated under the same conditions described above. On the following day, cells were treated with NAC-Ag_2S QDs at a concentration of 100 µg/mL for 1 h and fixed with paraformaldehyde solution (4% in PBS) for 20 min after being washed with PBS three times. Then, the fixed cells were stained with the nuclear dye DAPI (1 µg/mL) and left in 2 mL PBS to keep the cells against drying. Cells were visualized using an Olympus-Xcellence RT Life Science microscope (Olympus, Tokyo, Japan) equipped with filters for DAPI (λexc: 352-402 nm and λem: 417-477 nm) and for QDs (λexc: 550 nm and λem: 650 nm long-pass filter).

Images were colored and merged using the ImageJ software (version 1.46r, NIH, USA) [50]. Untreated cells were used as controls.

Determination of Apoptosis

Annexin-V staining was used to determine the apoptotic effect of NAC-Ag_2S QDs and equivalent free NAC (Supplementary Table 2) on MCF-7 cells. Cells were cultured as 1×10^5 cells/well in 6-well plates, treated with different concentrations of NAC-Ag_2S QDs (0.78–200 μg/ml) or free NAC (0.29-73.2 μg/ml) and incubated for 48 h. At the end of the treatment, cells were collected. Early/late apoptosis and cell death was determined by using Annexin V/Dead Cell kit (MCH100105, Millipore, Darmstadt, Germany) according to the manufacturer's instructions. The live, dead, early and late apoptotic cells were counted using a Muse Cell Analyzer (Millipore, Hayward, CA, USA) (n=3).

Induction of oxidative stress and ROS measurement

To evaluate the effect of different concentration of NAC-Ag_2S QDs (0.78–200 μg/ml) and equivalent free NAC (Supplementary Table 2) on ROS generation, a ROS kit (Cat no MCH 100111-2; Millipore) was employed according to the manufacturer's protocol. A Muse Cell Analyzer (Millipore, Bedford, MA, USA) was used for the analysis. The Muse® Oxidative Stress Kit determines the count and percentage of cells undergoing oxidative stress based on the intracellular detection of superoxide radicals. Obtained results were confirmed with the cell-permeant 2',7'-dichlorodihydrofluorescein diacetate (H2DCFDA) assay (Sigma, cat #D6883). H2DCFDA is a chemically reduced form of fluorescein and used as an indicator for reactive oxygen species (ROS) in cells. For this study, 5 x 10^3 cells were seeded into 96-well plates and incubated at 37°C under 5% CO_2

atmosphere The following day, cells were pretreated with 5 mM of DCFDA (dissolved in PBS) for 2h. Then, 5 mM of DCFDA and test material (NAC-Ag_2S QDs or free NAC) were simultaneously added to the cells. After 48 h incubation, emission from each well at 535 nm ($\lambda_{excitation}$=485 nm) was recorded using a micro-plate fluorometer (FLx800 Bio-Tek, Vermont, USA). The experiment was performed in triplicate in each plate and in duplicate plates.

γH2A.X assay for the assessment of DNA damage

MCF-7 cells were exposed to NAC-Ag_2S QDs (0.78–200 μg/ml) and free NAC (0.29-73.2 μg/ml) for 48 h (Supplementary Table 2), separately. After detachment with trypsinization, cells were centrifuged at 300 × g for 5 min, washed once with PBS and fixed with the Muse Fixation Buffer, which is a component of the Muse γH2A.X Activation Dual Detection kit (MCH200101, Millipore, Darmstadt, Germany) for 5 min on ice. Then, cells were permeabilized by ice-cold Muse Permeabilization Buffer and incubated on ice for 5 min. These cells were centrifuged (300 × g, 5 min), resuspended in 45 μL 1×assay buffer, and incubated with a mixture of 2.5 μL of antiphospho-Histone H2A.X and 2.5 μL of anti-Histone H2A.X, PECy5 for 30 min, in dark, at room temperature. At the end of the this incubation, cells were resuspended in 100 μL of 1×assay buffer, centrifuged (300 × g, 5 min) and resuspended in 150 μL of fresh 1×assay buffer. The levels of the Total protein and the phosphorylated H2A.X protein levels were measured using a Muse Cell Analyzer (Millipore, Hayward, CA, USA).

Statistical Analysis

Non-parametric Kruskall–Wallis one-way analysis of variance followed by multiple Dunn's comparison test of GraphPad Prism 6 software package (GraphPad Software, Inc., USA) was used for statistical analysis of the data. Comparison between two groups were performed using Mann-Whitney test. Only p-value < 0.05 was considered as statistically significant. All quantitative data were presented as mean values ± standard deviation (SD). All tests were two-tailed.

Results

Synthesis and characterization of NAC-Ag_2S QDs

NAC coated NIR emitting Ag_2S QDs were prepared in a single step directly in water using $AgNO_3$, Na_2S and NAC at pH 10 where NAC is fully deprotonated to provide stable nanoparticles (Supplementary Figure 1). After the addition of Na_2S to the reaction mixture, the color of the solution changed first to yellow-orange and then to brown. Variables, namely, Ag/S, Ag/NAC ratio, temperature and reaction time, were studied in detail to explore their effects on the particle properties including stability, size, emission wavelength and intensity. This allows determination of the best reaction recipe for the production of stable QDs with the strongest luminescence within the desired emission range and in small hydrodynamic sizes that are suitable for biomedical applications.

First, NAC amount was studied as an independent factor. NAC-Ag_2S were prepared at two different Ag/NAC mol ratio (1/2 (QD1) and 1/5 (QD4)) at fixed Ag/S ratio of 4/1 (Table 1). Increased amount of NAC resulted in formation of larger crystals with absorbance onset at longer wavelength than QD1 (Figure 1A-B, Table 1). QD4 have a broader full-width at half-maximum (FWHM) with emission maxima centered at 823 nm with slightly stronger emission intensity (Figure 1A). In order to test if larger crystal size

observed with higher concentration of NAC is a result of partial decomposition of NAC, a control experiment without Na_2S addition was performed (QD5) (Table 1). However, neither a color change in the reaction (18 h), nor luminescence were detected in the reaction mixture confirming that NAC does not release sulfur under these conditions.

Next, Ag/S mole ratio was studied to tune the crystal size further and hence, emission wavelength of QDs. Two different composition with Ag/S ratio of 4/1 (QD1) and 2/1 (QD2) at a fixed Ag/NAC ratio of 1/2 were synthesized at RT (Table 1). As shown in Figure 1A-B, decrease in Ag/S ratio increased the crystal size and resulted in a red shift of emission maxima to 840 nm with a slightly enhanced luminescence intensity compared to QD1 (emission maxima at 748 nm). Indeed, the reaction times indicated in Table 1 correspond to the time point where the strongest luminesce was obtained from that specific reaction. So, running the reaction closer to the stoichiometry provided faster reactions, as well, reducing the required time from 90 to 30 min.

Table 1. Influence of reaction conditions on the properties of NAC-Ag_2S QDs.

	QD1	QD2	QD3	QD4	QD5
Ag/S (mol/mol)	4/1	2/1	4/1	4/1	4/0
Ag/NAC (mol/mol)	1/2	1/2	1/2	1/5	1/5
T (ºC)	RT	RT	70	RT	RT
$\lambda_{abs(cutoff)}$[a] (nm)	683	795	719	778	ND
Size[b] (nm)	2.26	2.58	2.36	2.53	-
Band Gap (eV)	1.82	1.56	1.73	1.60	-

$\lambda_{em(max)}$ [c] (nm)	748	840	753	823	ND
FWHM (nm)	158	187	160	213	
time (min)	90	30	30	30	18h
QY (%)	NC	NC	33	NC	
D_h [d] (nm)	3.0 ± 1.3	2.6 ± 0.3	3.2 ± 1.0	NC	
Zeta potential (mV)	-41.6 ± 19.1	-51.4 ± 3.0	-35.3 ± 9.5	NC	

[a]Absorbance onset. [b]Calculated by Brus equation. [c] Emission maxima. [d] Hydrodynamic diameter measured by DLS and reported as the number average, NC : Not Calculated, ND : Not detected, RT : Room Temperature, FWHM : Full-width at half maximum of the emission peak.

Another variable that is influential in tailoring the crystal size and hence, the luminescence is the reaction temperature. Reactions with different Ag/S and Ag/NAC ratios were all performed at RT. Synthesis of QD1 was repeated at 70°C (QD3). This caused a faster reaction, a small increase in the crystal diameter (from 2.26 nm to 2.36 nm) and a small red shift in the emission maxima (from 748 nm to 753 nm) (Figure 1A and Table 1). Most dramatic impact of higher reaction temperature was seen in the luminescence intensity providing the most strongly luminescing NAC-Ag_2S QDs with 33% quantum yield (QY, with respect to LDS-798 NIR dye) (Supplementary Figure 2). Therefore, this composition was used in further characterization of QDs and in the *in vitro* studies.

Photoluminescence lifetime measurements conducted with QD3 indicated a multiexponential luminescence decay with an average lifetime ($T_{average}$) of 55.03 ns (Figure 2C). This is somewhat similar to lifetime values reported for other Ag_2S QDs with different coatings in the literature [23, 50]. The faster component (T1) which arises from non-radiative events such as surface dangling bonds or electron-hole traps, which are considered as defects, was determined as 8.40

ns. The major component in this case is (B2: 78%) the slower component (T2=67.85 ns), which arises from the desired electron-hole recombination.

The IR spectrum of NAC-Ag_2S QDs (QD3) were recorded between 4000-650 cm^{-1} and compared with the free NAC. Strong bands at 1587 and 1390 cm^{-1} are typical for asymmetric and symmetric carboxylate stretching modes of NAC and confirm its existence in the QD coating (Figure 1D). The disappearance of the S–H stretching band of NAC at 2550 cm^{-1} suggests the binding of NAC to Ag_2S core from its thiol group. The organic content of the QD3 was measured as 36.6% by Thermo Scientific Flash 2000 Organic Elemental Analyzer (Supplementary Table 1).

TEM analysis of NAC-Ag_2S QDs (QD3) indicates spherical nanoparticles with a size distribution between 1.45 nm and 5.20 nm (Figure 1E). EDX analysis of the nanoparticles shown in Supplementary Figure 3 confirmed the presence of Ag and S in QDs. Inter-planar distance of the crystalline structure was 0.22 nm which agrees with the reported values for the [031] plane of monoclinic Ag_2S (Figure 1F) [51, 52].

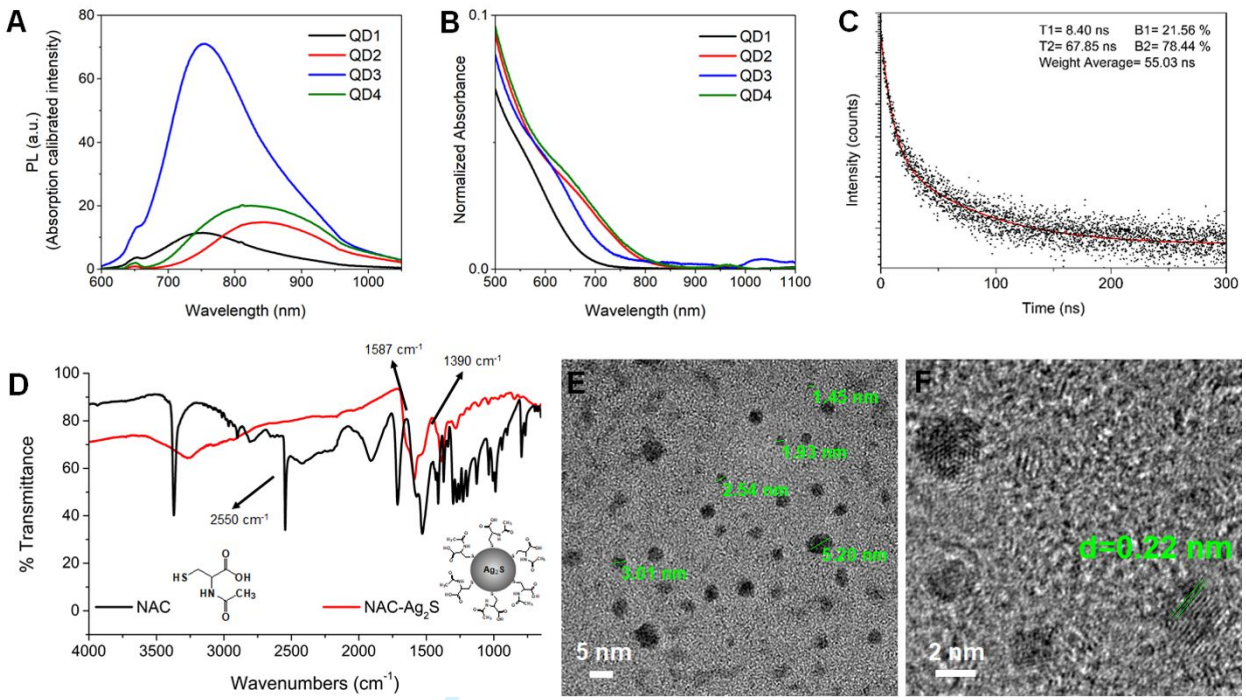

Figure 1. Characterization of NAC-Ag_2S QDs. (A) Photoluminescence and (B) absorbance spectra of NAC-Ag_2S QDs synthesized under different conditions summarized in Table 1. (C) Time resolved photoluminescence decay curve of NAC-Ag_2S (QD3). Black dots are scattered and red line is fitted data. B1 and B2 represent amplitudes of fast and slow components, respectively. (D) FTIR spectrum of free NAC and NAC-Ag_2S QDs, TEM images of the nanoparticles (E) at 5 nm scale and (F) focused lattice planes to determine the interplanar spacing and the corresponding plane.

Stability of NAC-Ag_2S QDs in different media

In order to investigate their stability, NAC-Ag_2S QDs (QD3) were suspended in a variety of biologically relevant media: dH_2O at pH 7.4 and 4.5, 10 mM NaCl, phosphate-

buffered saline (PBS) and fetal bovine serum (FBS). The hydrodynamic size and the charge of QDs in these media would influence the blood circulation time and biodistribution [53]. The luminescence intensity of NAC-Ag_2S QDs increases in FBS and PBS but no significant difference was observed in NaCl solution or at different pH values (pH 7.4 and 4.5) (Figure 2A). Absorbance of all these QD suspensions were identical except the FBS suspension which had a strong absorbance at 312 nm and a weak one at 435 nm (Figure 2B).

Hydrodynamic size and zeta potential of QDs in these media were determined immediately after the preparation of suspensions (0 hour) and after 2, 6, 12, 48 hours, to see if there is any precipitation or aggregation over time. The hydrodynamic size of the particles were quite similar in dH_2O pH7.4 (3.33 ± 0.34 nm), dH_2O pH4.5 (3.56 ± 0.90 nm), 10 mM NaCl (3.61 ± 0.34 nm) and PBS (3.69 ± 1.84 nm) at the initial time point (0 hour). QDs in FBS have larger average hydrodynamic size (5.85 ± 0.27 nm). There was no precipitation in the solutions over time and the hydrodynamic size stayed relatively constant (Supplementary Figure 4, Figure 2C). The zeta potential of the nanoparticles was measured at different time points, as well (Figure 2D). QDs had a negative zeta potential: -38.5 ± 6.8 mV in dH_2O pH7.4, -28.2 ±1.4 mV in 10 mM NaCl, -27 ± 6.2 mV in pH 4.5 dH_2O, -14.9 ± 3.8 mV in PBS, and -9.3 ± 0.7 mV in FBS indicating adsorption of the buffer or medium content on QDs in FBS and PBS. After 48 hours, zeta potentials were more negative: -66.7 ± 3.1 mV in pH7.4 dH_2O, -46.7 ± 0.2 mV in 10 mM NaCl, -45.6 ± 4.0 mV in pH4.5 dH_2O, -20.3 ± 1.1 mV in PBS and -10.1 ± 0.6 mV in FBS.

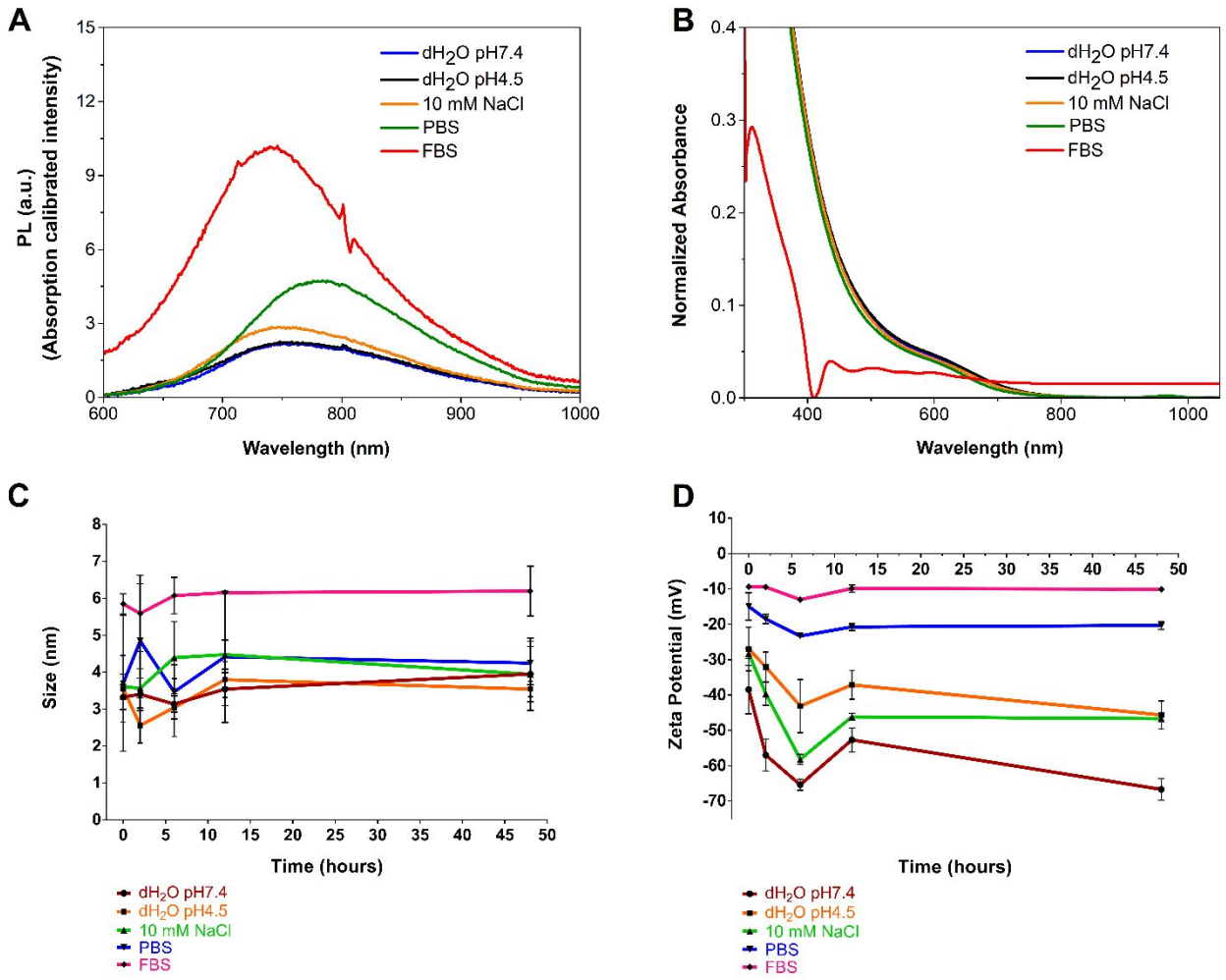

Figure 2. Influence of different media on photoluminescence (A), absorbance (B), hydrodynamic size (C) and zeta potential (D) of NAC-Ag_2S QDs.

In vitro anti-growth activity of free NAC and NAC-Ag_2S QDs

To evaluate the anti-growth effect of NAC-Ag_2S QDs (QD3), ATP viability assay was performed on MCF-7, HeLa, A549 and BEAS-2B cells after 24 h and 48 h incubation. NAC content of QD3 was determined by the Organic Elemental Analyzer and it was used for comparison in the experiments (Table S1). Concentrations of QD3 and the corresponding NAC amounts used in the *in vitro* studies are given in Table S2. As can be seen in Figure 3A and Figure 3B, free NAC did not affect the cell viability significantly,

whereas NAC-Ag_2S QDs effectively reduced cell viability in a time, dose and cell type dependent manner (Figure 3C and Figure 4D). The IC_{50} (half maximal inhibitory concentration) values were determined from the graphs in Figure 3A-D and summarized in Figure 3E. The most vulnerable cell line was determined as MCF-7 with an IC_{50} of 23.2 µg/mL in 24 h incubation which sharply decreased to 1.3 µg/mL in 48 h. HeLa required 63 and 14.8 µg/mL QD3 for IC_{50} in 24 and 48 h incubations, respectively. In case of BEAS-2B cells, 129 µg/mL QD3 was determined as IC_{50} but only after 48 h incubation. A549 cells responded differently to QD3: Only a slight decrease in the cell viability was seen in 24 h within the studied concentration range, which indeed became less after 48 h incubation.

For the rest of the *in vitro* studies, MCF-7 cell line was used since it emerged as the most sensitive cell type to NAC-Ag_2S QDs.

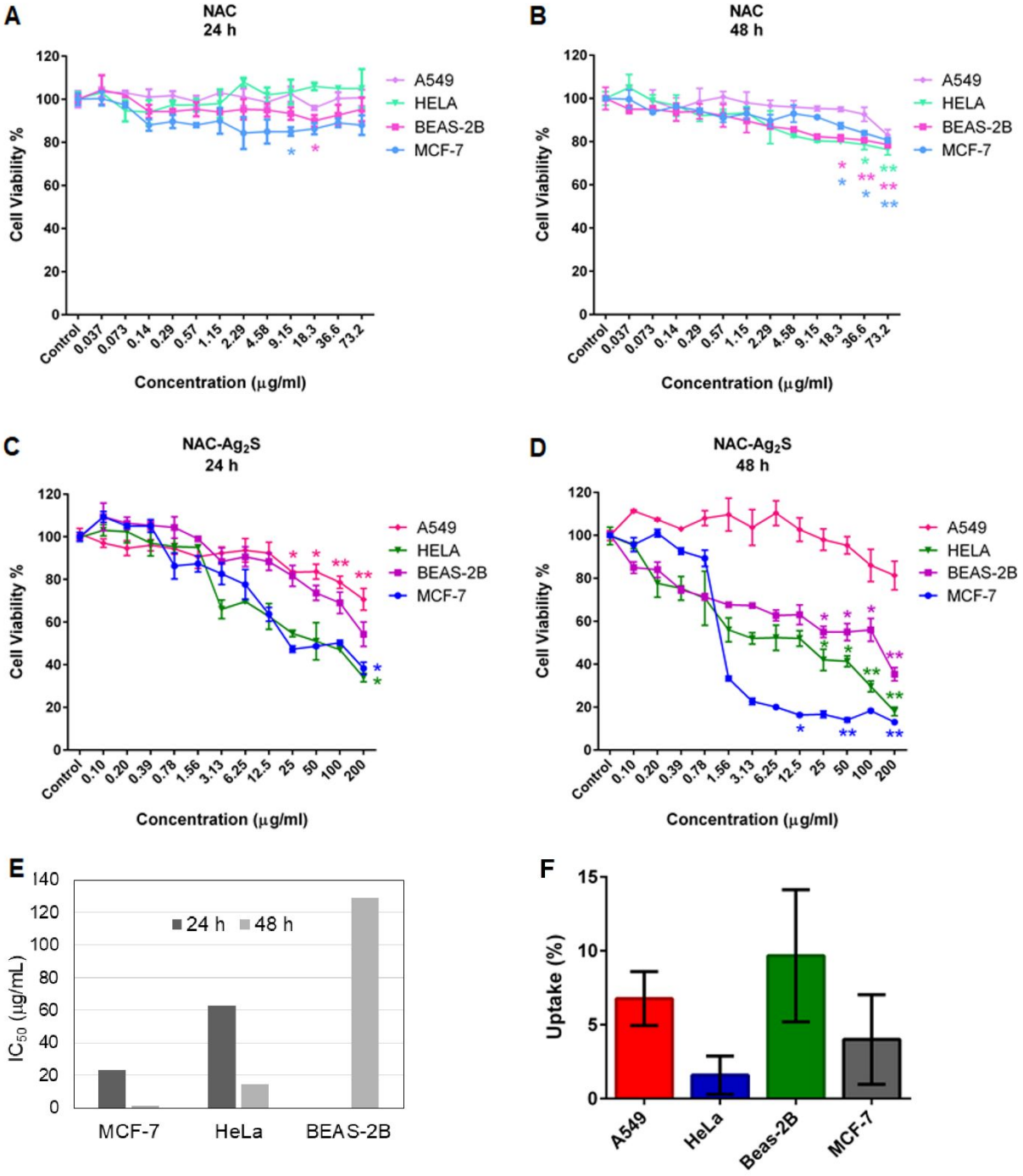

Figure 3. Cell viability of different cell lines treated with free NAC (A-B) and NAC-Ag_2S QDs (C-D) determined by ATP assay 24 h and 48 h after exposure. Data are expressed as mean ± SD. * denotes statistically significant differences in comparison with control: * ($p<0.05$) and ** ($p<0.01$), (n = 3). (E) IC_{50} values of NAC-Ag_2S QDs in different cell

lines after 24 and 48 h incubation. (F) Intracellular quantification of NAC-Ag_2S QDs in different cell lines by inductively coupled plasma-mass spectrometry (ICP-MS). QDs at 100 μg/mL concentration were incubated with cells for 1 h. The data are expressed as mean ± SD (n = 4).

Intracellular uptake of NAC-Ag_2S QDs and optical imaging

Internalization of QDs by these different cell lines was determined quantitatively from the intracellular Ag ion concentration using ICP-MS and qualitatively by fluorescence microscope equipped with a NIR filter set. Cells were treated with 100 μg/mL of NAC-Ag_2S QDs for 1 hour. For the ICP-MS measurements, they were detached and digested by an acid treatment. For the optical imaging, they were fixed and investigated under the microscope. Based on the intracellular Ag concentrations, BEAS-2B (human bronchial epithelial cells) and A549 (a cancer cell line of lung) showed the highest QD internalization. Interestingly, these two cell lines showed the highest viability when treated with NAC-Ag_2S QDs. MCF-7 and HeLa cells internalized QDs in much lower amount. . HeLa showed the least QD uptake (Figure 3F).

Internalization of QDs by these cells was also confirmed using fluorescence microscopy (Figure 4). Luminescence of QDs can be clearly noticed by NIR signal detected in the cytoplasm of the cells. This indeed indicates that NAC-Ag_2S QDs are promising optical imaging probes. The most intense optical signal was detected in BEAS-2B cells and the lowest emission was observed in HeLa cells, which is in agreement with

the ICP-MS results. This suggests that NAC-Ag_2S QDs may be a selective theranostic nanoparticle for some cancer types.

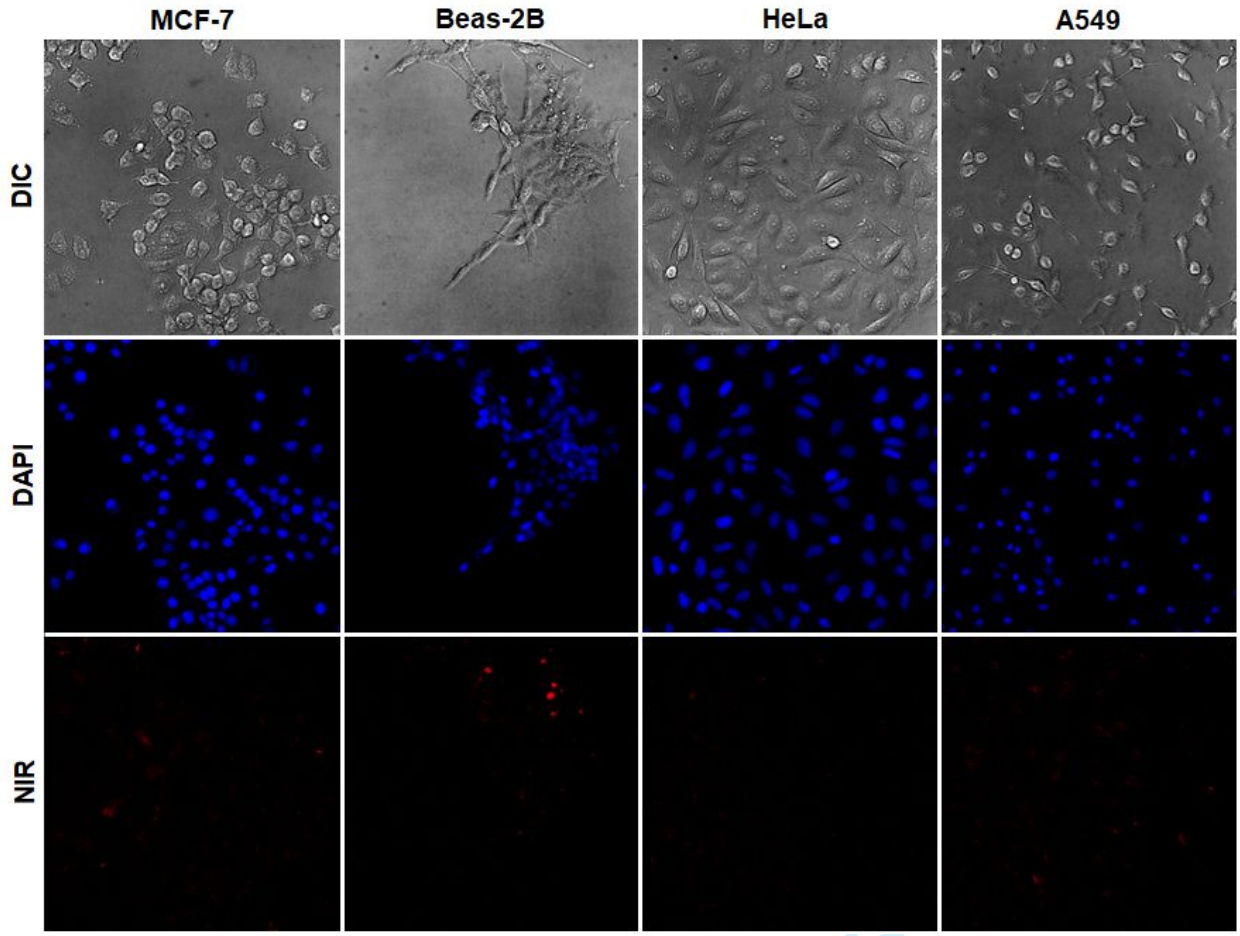

Figure 4. Fluorescent microscopy images of MCF-7, Beas-2B, HeLa and A549 cells after 1 h incubation with NAC-Ag2S QDs at 100 μg/ml concentration. DIC: differential interference contrast; DAPI: 4′,6-diamidino-2-phenylindole; NIR: Near-infrared images. Blue emission shows DAPI nuclear staining and red emission originates from emission of QDs.

Apoptosis-inducing effect of NAC-Ag_2S QDs

Significantly reduced cell viability of MCF-7 cells by NAC-Ag_2S was investigated further. The apoptotic potential of NAC-Ag_2S QDs (0.78–200 μg/ml) and equivalent free NAC (0.29-73.2 μg/ml) were evaluated by using Annexin V/Dead Cell assay in MCF-7 cell line (Figure 5 and Supplementary Figure S5). Cells treated with free NAC showed a very high fraction of live cells in the entire concentration range with no significant dose dependence: 90.60% live cells at 0.29 μg/ml and 89.10% at the highest concentration (73.2 μg/ml). On the other hand, fraction of live cells are 31.60% even at the lowest concentration (0.78 μg/ml) and 2.70% at the highest concentration (200 μg/ml) of NAC-Ag_2S QDs. Rest of the cells are either in the early and late apoptotic stage or dead. Overall, NAC-Ag_2S QDs increases the percentage of total apoptotic MCF-7 cells that were mainly in the late apoptosis, which increases further with the increasing dose. For example, 13.85% of the cells are dead, 52% are late apoptotic/dead and 2.55% are early apoptotic cells at 0.78 μg/ml concentration of NAC-Ag_2S QDs, while these numbers are 53.15%, 44% and 0.15% at 200 μg/ml QD.

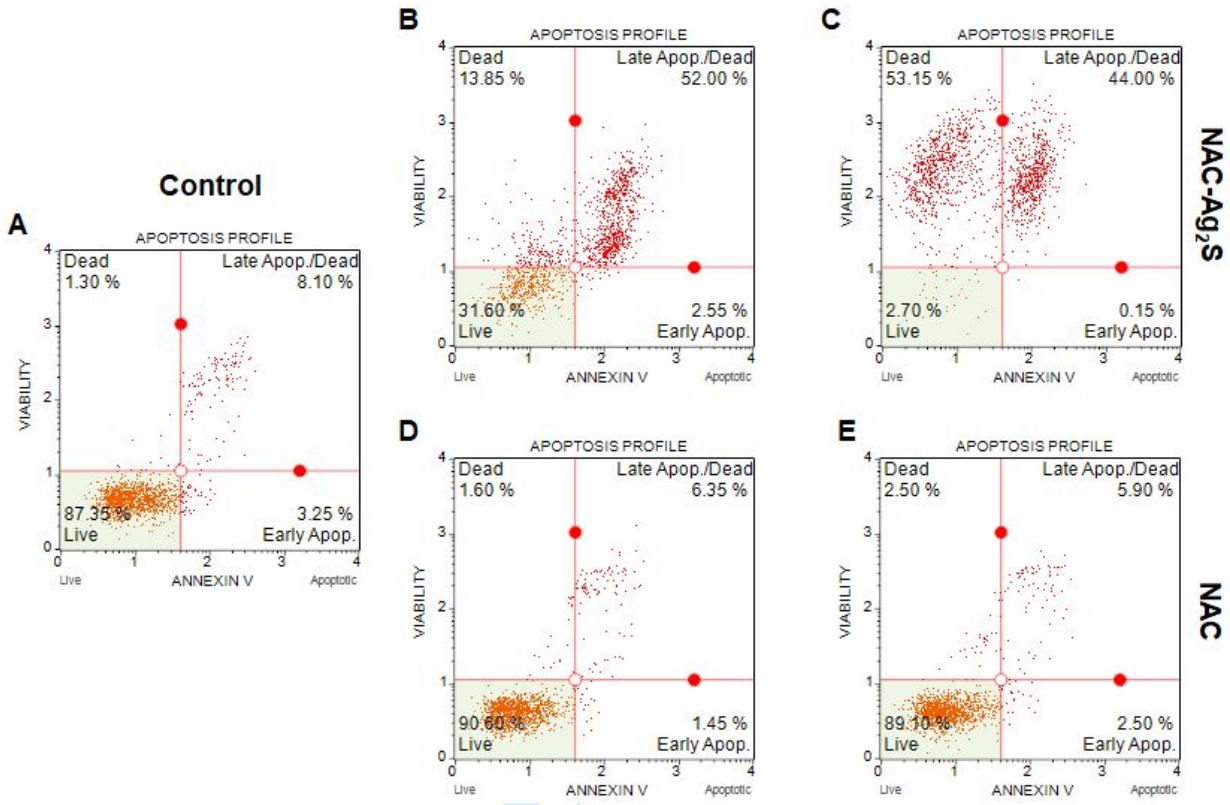

Figure 5. Determination of apoptosis in MCF-7 cells treated with NAC-Ag_2S QDs (B-C) or free NAC (D-E) for 48 h and assessed by Annexin V/Dead Cell assay using flow cytometry. Percentages of cells were presented in each quadrant. (A) Control; (B) 0.78 µg/mL and (C) 200 µg/mL of NAC-Ag_2S QD; (D) 0.29 µg/mL and (E) 73.2 µg/mL of free NAC treated cells.

ROS downregulation of NAC-Ag_2S QDs

Since ROS is usually associated with apoptosis, and NAC is a well-known antioxidant and free radical scavenger, the influence of NAC-Ag_2S QDs and free NAC on ROS levels was studied with two independent assays in a broad concentration range (0.78-200 µg/ml).

First, a standard ROS kit was used and intracellular ROS levels were determined by flow cytometer. In the results shown in Supplementary Figure S6, "M2" represents the

percentage of cells with an increased production of ROS. When compared with the control, there are significant reductions in the ROS level at 100 and 200 µg/mL QD. M2 values drop down to 2-5% from 10%, respectively. Influence of free NAC on the ROS level is not as significant as in the case of QDs, but there is some fluctuation in the data. So, a second method, DCFDA assay which uses a cell permeable fluorescent reagent, 2',7'-dichlorofluorescin diacetate, was used to measure the ROS level [54]. This method also confirms that NAC-Ag_2S QDs decrease the ROS amount in MCF-7 cells at and above 50 µg/ml concentration while no significant ROS reduction was seen with free NAC within the studied dose range (0.037-73.2 µg/mL) (Figure 6). So, conjugation of NAC onto nanoparticles increases its ROS scavenging effect.

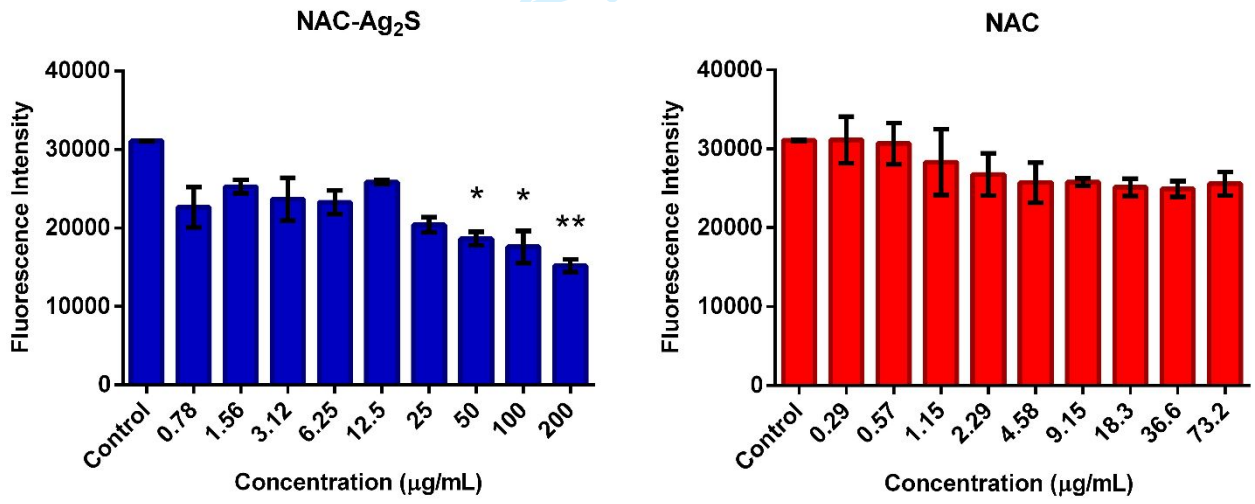

Figure 6. ROS downregulation by NAC-Ag_2S QDs and equivalent free NAC in MCF-7 cells measured by DCFDA assay 48 h after the exposure. Data represents mean ± SD of three independent experiments ($p < 0.05$ (*), $p < 0.01$ (**)).

DNA damage

The DNA damage in MCF-7 cells caused by NAC-Ag_2S QDs and free NAC was evaluated by γH2A.X assay 48 h after treatment. As shown in Figure 7 and Supplementary Figure S7, H2A.X phosphorylation increases in a dose-dependent manner upon NAC-Ag_2S QD exposure. The damage observed with free NAC appears to be much lower than NAC-Ag_2S. γH2A.X levels (shown as activated cells in Figure 7 and Supplementary Figure S7) in the NAC treated cells were between 4.5-16.5% in the whole concentration range while it increased to 17.40 - 66% in the QD treated cells. For the control cells , γH2A.X level was about 5.6%.

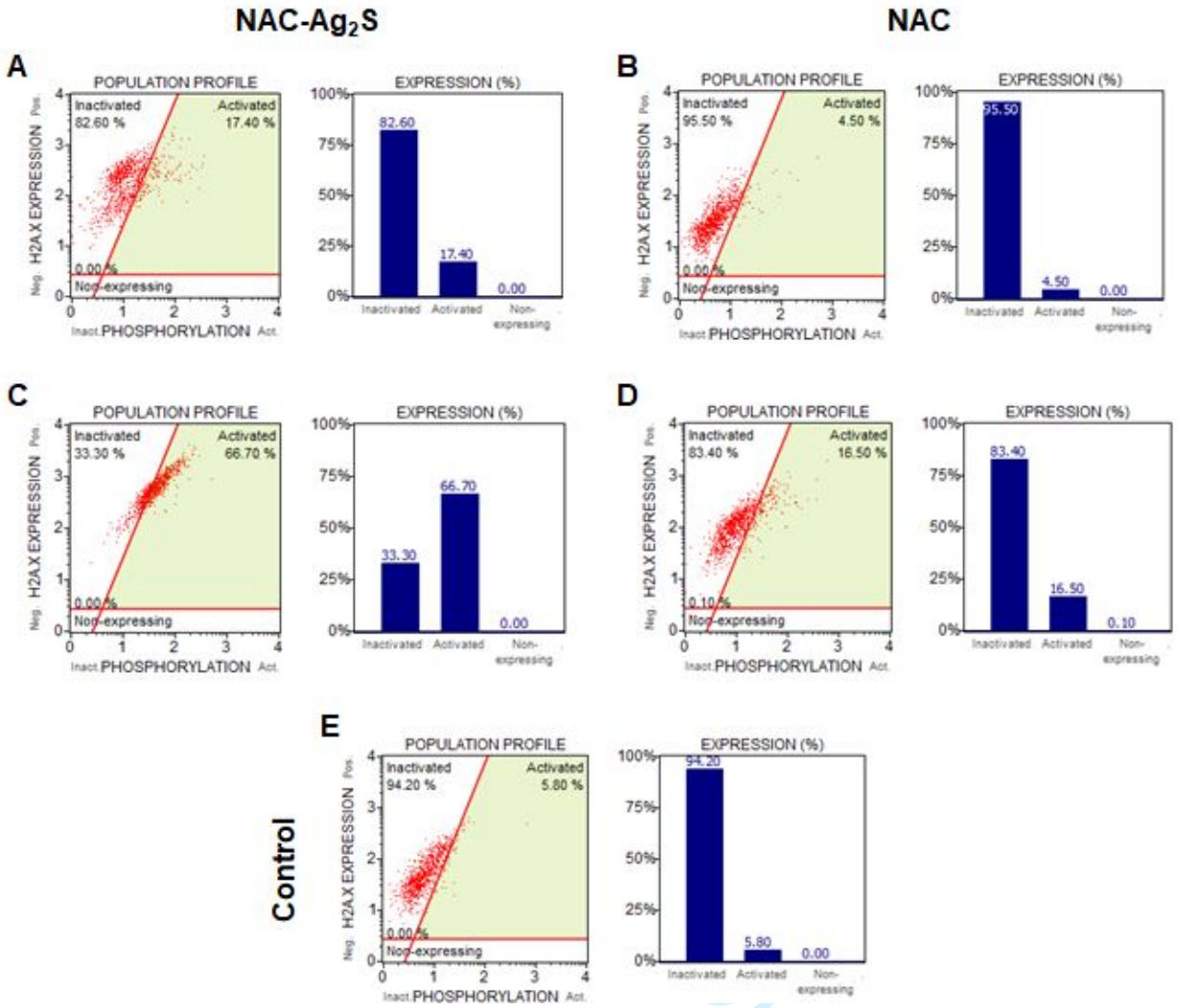

Figure 7. γH2A.X levels in MCF-7 cells treated with NAC-Ag_2S QDs (A and C) and NAC (B and D) measured by flow cytometry 48 h after treatment. (A) 0.78 µg/mL and (C) 200 µg/mL of NAC-Ag2S QD; (B) 0.29 µg/mL and (D) 73.2 µg/mL of free NAC treated; and (E) control cells.

Discussion

Through a thorough study of reaction variables, an optimized recipe for the production of strongly luminescent Ag_2S-NAC QDs with emission in the medical imaging window, small hydrodynamic size and stability in biologically relevant media was determined.

Synthesis of Ag_2S-NAC QDs at Ag/S ratio of 4/1, NAC/Ag ratio of ½ at 70°C and pH 10, produced QDs with strong emission centered at 753 nm (FWHM=160 nm) with 33 % quantum yield, strong negative surface charge (-35.3 ± 9.5 meV) and small (3.2 ± 1.0 nm) hydrodynamic size. By changing the variables, QDs with emission maxima between 748-840 nm were obtained. All produced particles are small, have a negative surface charge with zeta potential between ca -52 to -35 mV and all are colloidally stable.

The first reaction variable studied was the coating (NAC) amount. Increasing the NAC amount in the reaction from Ag/NAC ratio of 1/2 (QD1) to 1/5 (QD4), in otherwise identical conditions, caused production of larger crystals (2.26 nm versus 2.53 nm) exhibiting a red shift in emission maxima from 748 nm to 823 nm with a broader emission peak (FWHM 158 versus 213 nm) (Table 1 and Figure 1A-B). Time required to achieve the strongest emission from the particles produced at higher NAC concentration was 30 min versus 90 min at low NAC concentration (Table 1) indicating a faster nucleation and growth at higher NAC concentration. Such increasing crystal size and faster growth kinetic may be due to the release of extra sulfur in case of decomposition of the coating molecule which would decrease the Ag/S ratio and the effective concentration of the coating material. Both of these would increase the crystal size. However, control reaction run in the absence of a sulfur source did not produce any Ag_2S in 18h confirming that NAC does not decompose and change the stoichiometry of the reaction (QD5) but act only as a coating material. Increasing amount of NAC in the reaction mixture may cause a crowding on the crystal surface or enhance intramolecular interactions limiting the earlier passivation of the growing crystal.

Ag/S ratio is usually one of the major factors determining the crystal size. Decreasing Ag/S ratio from 4 (QD1) to 2 (QD2) shifted the emission maxima from 748 nm to 840 nm with a

slightly enhanced luminescence intensity (Figure 1A). Running reactions closer to the stoichiometry speeded up the kinetics (30 min versus 90 min) and produced larger crystals as expected with a band gap reduced from 1.82 eV to 1.56 eV corresponding to 2.26 and 2.58 nm crystals, respectively (Table 1).

Reaction temperature affects the growth kinetics of nanoparticles and therefore, is another critical factor in controlling the crystal size and emission wavelength. All these reactions were performed at room temperature but when the recipe of QD1 was run at 70°C (QD3), slightly larger crystals (2.26 nm versus 2.36 nm) with a dramatically stronger emission at slightly longer wavelength (753 nm) were obtained in shorter reaction times (30 min) (Figure 1A and Table 1). As the temperature increases the stable crystal size increases as well, resulting in formation of larger crystals. At the same time, at higher growth temperature, better crystallization and mobility of surface atoms may provide a better quality of crystal surface with less surface defects, reducing the defect related non-radiative relaxation of the photogenerated electron and hole. This improves the emission intensity.

In this study, all produced particles were small, had a negative surface charge with zeta potential between ca -52 to -35 mV and were all colloidally stable (Table 1). Since NAC has a free carboxylic acid group, negatively charged QDs were expected. Therefore, all further characterization of QDs and the *in vitro* evaluations were performed with the most strongly luminescent NAC-Ag_2S (QD3) with 33% quantum yield.

Coating of QDs are not only important in controlling the crystal size and colloidal stability but also, for luminescence properties. Dense and strong binding of the coating molecules on crystal surface eliminates surface defects, which are usually the major cause of weak

luminescence. Thiol containing structures like NAC show high binding affinity to crystal surface through their thiol groups and provide stable particles. Luminescence lifetime measurements indicated a multiexponential decay with the major contribution of the slower decay component (T2=67.85 ns) which is attributed to the electron-hole recombination rather than surface defects (Figure 1C). This finding supports the high quantum yield of these QDs.

Effective surface passivation was further supported by the FTIR analysis. Absence of –SH stretching band of NAC at 2550 cm^{-1} along with the presence of typical carboxylate stretching peaks confirmed the presence of NAC, absence of free NAC and binding of NAC to Ag_2S crystal from its thiol group (Figure 1D). Well passivated and stabilized QDs with strong negative surface charge had quite small hydrodynamic size in agreement with the crystal sizes calculated from the Brus equation (2.26-2.58 nm) and sizes measured from TEM images (1.45-5.20 nm) (Figure 1E and Table 1). TEM images also prove crystalline, monoclinic Ag_2S core with inter-planar distance of 0.22 nm (Figure 1F).

Both colloidal and luminescence stability of the QDs in biologically relevant media have a crucial importance for practical applications. The hydrodynamic size and the surface charge influence the blood circulation time and biodistribution of nanoparticles [53]. Hence, size, charge and luminescence of NAC-Ag_2S QDs in dH_2O at pH 7.4 and 4.5, mimicking the plasma and intracellular pH values, 10 mM NaCl and phosphate-buffered saline (PBS) which are common diluents for in vitro and in vivo studies and fetal bovine serum (FBS) which is a supplement in cell culture medium providing a combination of biologically relevant mixture of growth factors, proteins, vitamins, etc., were measured (Figure 2). In a period of 48h, QDs stayed colloidally stable in each of these media and the hydrodynamic size stayed relatively constant with negative surface charge supporting the colloidal stability provided by electrostatic repulsion of particles.

Measurements were conducted at different time points with 48 h as the end point. This is mainly because 24 h and 48 h are comment incubation times in the in vitro studies and, in the in vivo studies 48h is usually enough for major organ distribution. The strong negative zeta potential at pH 7.4 decreased at pH 4.5 due to partial protonation and in 10 mM NaCl due to some shielding in charge repulsion. However, in all of the studied media, QDs were negatively charged and provided colloidal stability (Supplementary Figure S4).

NAC has been reported to inhibit growth, proliferation and invasive behavior of human cancer cells, including colorectal [55], bladder [56, 57], prostate [58], tongue [59] and lung [60] carcinoma *in vitro*. Hence, first a dose dependent viability test was performed on MCF-7, HeLa, A549 and BEAS-2B cells after 24 h and 48 h incubation with QDs. ATP assay is a bioluminescence assay that uses recombinant firefly luciferase enzyme in order to quantify the amount of cellular ATP in the viable, metabolically active cells and gives more realistic results compared to frequently used MTT assay [61]. Results were compared with free NAC at the concentrations corresponding to the NAC content of QD3 (Figure 3A-B). NAC-Ag_2S reduced cell viability more dramatically in MCF-7 and HeLA cells in a dose and time dependent manner with IC50 values of 23.2 and 63 µg/mL in 24 h, and 1.3 and 14.8 µg/mL in 48 h, respectively (Figure 3C-E). Lung derived cells behaved quite differently. There was no significant reduction in the viability of BEAS-2B cells in 24 h. Toxicity was observed after 48 h with a quite high IC_{50} value of 129 µg/mL. A549 cells seemed to be more vulnerable in 24 h than in 48 h exposure. At longer incubation times, cells might have developed some resistance to NAC-Ag_2S QDs. However, in either case, even at the highest (200 µg /mL) QD concentration viability of A549 cells was above 50%. Free NAC at the corresponding concentrations did not induce significant toxicity in any of the cell lines in 24 h. However, up to 20% reduction in cell viability was seen

only at the highest three concentrations (18.3-73.2 μg /mL) after 48 h incubation (Figure 3A-B). Enhanced cytotoxicity or reduced cell viability at higher dose of QDs and/or longer exposure time is most probably related to increased uptake and time dependent intracellular kinetics. Overall, these findings imply that although NAC has no significant cytotoxicity to these cell lines, NAC-Ag_2S QDs may induce significant toxicity in breast and cervical cancer cells. It is notable that cancerous or healthy lung cells behave differently and A549 cells are not significantly affected by NAC-Ag_2S QDs.

It is important to evaluate such viability results along with the intracellular concentration of QDs. Based on the intracellular Ag concentrations measured by ICP-MS, BEAS-2B and A549 internalized more QDs than MCF-7 and HeLa cells in this given order (Figure 3F). These measurements were done after 1h incubation of the cells with QDs in order to have 100% cell viability, so that we would not lose the dead cells with may be more QD loading. The highest uptake was about 10 % of the loaded dose (100 μg/mL QD). Interestingly, BEAS-2B and A549 cells showed the highest viability despite of the higher uptake, which indicates a significant cytocompatability of these QDs in these lung derived cell lines. MCF-7 and HeLa cells internalize much less QDs (in the order of 4.5 and 2%) but are the more vulnerable ones, which indicates significant cytotoxicity of NAC-Ag_2S QDs in these cell lines.

Fluorescence images of the cells treated with QDs indicate cytoplasmic distribution of QDs in each cell line (Figure 4). BEAS-2B cells with the highest amount of QD load provided a very strong optical image but HeLa cells with low level of QDs showed a very weak NIR signal, which is in agreement with the internalization data. Selective uptake coupled with selective toxicity may provide numerous opportunities in the utilization of NAC-Ag_2S QDs as a selective theranostic nanoparticle for certain cancer types.

While NAC was usually used to reverse or reduce the ROS based toxicity of QDs in the literature, it is also reported to have pro-apoptotic effects on cancer cells. For instance, Amini et al. demonstrated cell cycle inhibition and induction of apoptotic cell death by NAC in the gastrointestinal carcinoma cells [62]. Nargi et al. reported a similar involvement of NAC in cell cycle arrest or apoptosis in a range of colorectal cancer (CRC) cell lines [55]. Guan et al. suggested that NAC induces apoptosis via endoplasmic reticulum stress and unfolded protein response pathways in HeLa cells [63]. In several other studies, NAC was reported to induce apoptosis in aortic smooth muscle cells or p53-mediated apoptosis in several oncogenically-transformed fibroblasts but not in endothelial cells or in normal cells [64-66]. Therefore, the apoptotic cell death caused by NAC-Ag_2S QDs was evaluated in the full concentration range of 0.78–200 μg/ml by using Annexin V/Dead Cell assay in the most vulnerable MCF-7 cell line (Figure 5 and Supplementary Figure S5). It is clear that as the concentration of QDs increases, the amount of apoptotic cells increases, and at the highest concentration (200 μg/ml) 53.15% of the cells were dead, 44% were late apoptotic/dead and 0.15% were early apoptotic cells. Major changes seems to occur between 3-6 μg/ml and 50-100 μg/ml doses (Supplementary Figure S5). These results clearly indicate that NAC-Ag_2S QDs induce a dose dependent apoptosis in MCF-7 cells while about 90% of cells were live in the whole concentration range (0.037-73.2 μg/mL) of free NAC. Choi et al. showed significant toxicity of NAC capped or NAC conjugated CdTe on human neoroblastoma cells at the dose of 5 μg/mL in 24 h [36]. However, they claim that NAC-CdTe has lower cellular uptake and hence are less toxic compared to cationic cysteamine coated CdTe. The IC_{50} values for the four cell lines studied here are much higher than this concentration. So, in a way NAC-Ag_2S is much safer than NAC-CdTe, at least partially due to Cd-free nature.

ROS is a very important factor associated with apoptosis and NAC is a well-known antioxidant and free radical scavenger. Therefore, it has been used to reverse the QD based toxicity in the literature. In two different methods used for the determination of ROS levels in MCF7 cells exposed to QDs or free NAC, it was clearly seen that NAC-Ag_2S QDs reduced ROS level much more effectively than free ROS, especially above 50 µg/ml concentration (Figure 6). Typically, NAC is used between 0.0408-1.306 mg/mL (0.25 mM-8 mM) concentration range for suppression of ROS in the literature [43, 67]. Here, the studied dose of free or bound NAC is 0.037-73.2 µg/mL. So, conjugation of NAC onto nanoparticles increases its ROS scavenging effect probably by improving its uptake as also shown in other reports [43, 49, 67]. This is interesting since NAC-Ag_2S lacks free sulfhydryl group, and QDs were stable in lysosomal pH. Downregulation of ROS along with the enhanced apoptosis in MCF-7 cells may be supported by some reports on reduced ROS production and Akt phosphorylation by NAC in breast cancer cells, resulting in apoptotic cell death [42] and NAC associated enhancement of H_2O_2, UV and MK886 induced apoptosis of murine hybridoma [68], human melanoma [69] and human T-cell leukemia cells [70].

Another route for cell death is DNA damage, which was studied by γH2A.X assay in this study. Elevated levels of γH2A.X (shown as activated cells in Figure 7 and Supplementary Figure S7) in the QD treated MCF7 cells (17.40 – 66 %) compared to NAC treated cells (4.5-16.5 %) and the control (5.8 %) indicates that NAC-Ag_2S causes a significant DNA damage compared to free NAC. This suggest that the DNA damage is ROS independent. There are many studies demonstrating that ROS is not required for DNA damage [71, 72].

Conclusion

In this study, we present a simple, one-step aqueous synthesis and detailed characterization of NAC-Ag_2S QDs. NAC is bound to the crystal surface via S-Ag bonds providing stable nanoparticles. By varying the synthetic recipe, the wavelength of the emission maxima was tuned between 750-840 nm, which is within the recommended optical imaging window. The most luminescent composition have 33% QY. QDs have ultrasmall hydrodynamic size, which is valuable for further functionalization and prolonged blood circulation. All QDs have strong negative surface charge and excellent colloidal and optical stability in different, biologically relevant media and pH values including the physiological pH and endosomal acidic pH.

NAC-Ag_2S QDs were well internalized by several different cell lines, MCF-7, HeLa, A549 and BEAS-2B and generated a significant intracellular signal proving its potential as an optical imaging agent or a luminescent label.

In vitro cytotoxicity evaluation of NAC-Ag_2S QDs in these four different cancerous or healthy cells in a broad concentration range (0.1-200 μg/ml corresponding to 0.037-73.2 μg/ml free NAC) showed that NAC-Ag_2S QDs reduce viability of MCF-7 and HeLa cells significantly while free NAC did not induce much cell death. This is quite an interesting result and should originate from the NAC coating since Ag_2S coated with different materials such as 2MPA or DMSA showed no toxicity to similar cells (MCF7 and HeLa) even at much higher doses [16, 21]. It is quite interesting that such high cytoctoxicity to MCF7 and HeLa cells is not correlated with higher cellular uptake since A549 and BEAS-2B internalized more QDs but were not affected as much as the other

tumor cell lines. A549 seems to be quite resistant and toxicity was seen in BEAS-2B mostly after 48h. In fact, this differential cytotoxic activity on different tumor types is highly desirable for an anticancer agent since it indicates organ/tissue-specific activity of QDs. Therefore, NAC-Ag_2S QDs may be a good candidate for an investigational new drug (IND). Indeed, higher uptake by lung based cells coupled with lower toxicity to these cell lines is also interesting and deserves further investigation by experts in the field. Lung cells (normal or cancerous) may have higher level of oxidative stress, which results in the utilization of NAC more rapidly compared to the breast or cervix cells. Indeed, NAC is used in obstructive pulmonary disease to reduce symptoms and exacerbations as an adjunct therapy [73, 74]. It is reported for activity in lung cancer prevention, as well [75]. This may be due to its antioxidative (or unknown) properties because oxidation is known to damage DNA that results in mutations, thereby cancer, over time.

Further studies performed with the most sensitive cell line, MCF-7, showed that NAC-Ag_2S QDs suppress ROS level, even more effectively than free NAC, and trigger DNA damage-induced apoptosis. This is also interesting considering that NAC is conjugated to nanoparticles from the thiol units, which has the primary role in radical scavenging. One example in the literature, which states significant toxicity of NAC-CdTe in neuroblastoma cells did not specify the origin of such toxicity [36]. This needs further investigation, which is beyond the scope of the current study.

Overall, in this study, not only highly stable and strongly luminescent NAC-Ag_2S QDs were developed, but also its potential as a theranostic QD in selected cancer cells/types was discovered.

Future Perspective

NAC coated Ag_2S is produced for the first time and in vitro cytotoxicity studies revealed that NAC does not render QDs non-toxic for each and every cell line. Its safety is dose and cell type dependent. This should encourage researchers, who uses biomolecules as safe coating alternatives, to perform their studies in a broader dose range with a wider selection of cell lines. Besides, selective uptake and cytotoxicity of these QDs is quite unexpected hence, will initiate a new research to investigate the origin of this selectivity and its utilization for lung cancer. Considering that 2D cell studies are actually not perfect models to make firm conclusions, we plan to investigate their selectivity and theranostic potential with animal studies.

Summary Points

- The main aim of this study is to develop NIR emitting NAC coated aqueous Ag_2S QDs as optical imaging and therapeutic agent.
- We demonstrated for the first time the synthesis of highly stable, NAC coated Ag_2S QDs with a strong emission tunable between 748-840 nm with quantum yield as high as 33%.
- NAC coated Ag_2S QDs have small hydrodynamic sizes and strong negative surface charge as well as excellent colloidal and optical stability in different media and pH values.
- *In vitro* cytotoxicity studies performed in a broad dose range (upto 200 □g/mL QD) showed that although NAC is not toxic, NAC-Ag_2S QDs may be quite toxic.

- In the *in vitro* studies NAC-Ag_2S QDs showed selective toxicity in human breast cancer (MCF-7) and cervical cancer (HeLa) cell lines compared to lung adenocarcinoma (A549) and bronchial epithelial (BEAS-2B) cells.
- NAC-Ag_2S QDs were internalized more by A549 and BEAS-2B cells than MCF-7 and HeLa cells but were not as toxic to lung based cells.
- Detailed *in vitro* studies on the most sensitive cell line, MCF-7, demonstrated that NAC-Ag_2S QDs suppress ROS level even more than free NAC.
- NAC-Ag_2S QDs trigger DNA damage-induced apoptosis in MCF-7 cell line.
- NAC-Ag_2S QDs generated a strong intracellular signal in NIR region of optical spectrum and proved their potential as an effective optical imaging agent.
- NAC-Ag_2S QDs emerged as a good candidate for an investigational new drug with diagnostic potential.

Financial & competing interests disclosure

The authors have no other relevant affiliations or financial involvement with any organization or entity with a financial interest in or financial conflict with the subject matter or materials discussed in the manuscript apart from those disclosed.

No writing assistance was utilized in the production of this manuscript.

References

1. Resch-Genger U, Grabolle M, Cavaliere-Jaricot S, Nitschke R, Nann T. Quantum dots versus organic dyes as fluorescent labels. *Nat. Methods* 5(9), 763 (2008).
2. Bruchez M, Moronne M, Gin P, Weiss S, Alivisatos AP. Semiconductor nanocrystals as fluorescent biological labels. *Science* 281(5385), 2013-2016 (1998).
3. Medintz IL, Uyeda HT, Goldman ER, Mattoussi H. Quantum dot bioconjugates for imaging, labelling and sensing. *Nat. Mater.* 4(6), 435 (2005).
4. Klohs J, Wunder A, Licha K. Near-infrared fluorescent probes for imaging vascular pathophysiology. *Basic Res. Cardiol.* 103(2), 144-151 (2008).
5. Altınoğlu Eİ, Adair JH. Near infrared imaging with nanoparticles. *Wiley Interdiscip. Rev. Nanomed. Nanobiotechnol.* 2(5), 461-477 (2010).
6. Hilderbrand SA, Weissleder R. Near-infrared fluorescence: application to in vivo molecular imaging. *Curr. Opin. Chem. Biol.* 14(1), 71-79 (2010).

- **It is a review of in vivo applications of near-infrared fluorescence imaging with improved photon penetration through tissue and minimal tissue autofluorescence.**

7. Chen H, Wang Y, Xu J *et al*. Non-invasive near infrared fluorescence imaging of CdHgTe quantum dots in mouse model. *J. Fluoresc.* 18(5), 801-811 (2008).
8. Qian H, Dong C, Peng J, Qiu X, Xu Y, Ren J. High-quality and water-soluble near-infrared photoluminescent CdHgTe/CdS quantum dots prepared by adjusting size and composition. *J. Phys. Chem. C* 111(45), 16852-16857 (2007).
9. Liang G-X, Gu M-M, Zhang J-R, Zhu J-J. Preparation and bioapplication of high-quality, water-soluble, biocompatible, and near-infrared-emitting CdSeTe alloyed quantum dots. *Nanotechnology* 20(41), 415103 (2009).
10. Deng D, Xia J, Cao J *et al*. Forming highly fluorescent near-infrared emitting PbS quantum dots in water using glutathione as surface-modifying molecule. *J. Colloid Interface Sci.* 367(1), 234-240 (2012).
11. Chen N, He Y, Su Y *et al*. The cytotoxicity of cadmium-based quantum dots. *Biomaterials* 33(5), 1238-1244 (2012).
12. Su Y, Hu M, Fan C *et al*. The cytotoxicity of CdTe quantum dots and the relative contributions from released cadmium ions and nanoparticle properties. *Biomaterials* 31(18), 4829-4834 (2010).
13. Du Y, Xu B, Fu T *et al*. Near-infrared photoluminescent Ag2S quantum dots from a single source precursor. *J. Am. Chem. Soc.*132(5), 1470-1471 (2010).
14. Hong G, Robinson JT, Zhang Y *et al*. In vivo fluorescence imaging with Ag2S quantum dots in the second near-infrared region. *Angew. Chem.* 124(39), 9956-9959 (2012).
15. Duman FD, Hocaoglu I, Ozturk DG, Gozuacik D, Kiraz A, Acar HY. Highly luminescent and cytocompatible cationic Ag 2 S NIR-emitting quantum dots for optical imaging and gene transfection. *Nanoscale* 7(26), 11352-11362 (2015).
16. Hocaoglu I, Cizmeciyan MN, Erdem R *et al*. Development of highly luminescent and cytocompatible near-IR-emitting aqueous Ag 2 S quantum dots. *J. Mater. Chem.* 22(29), 14674-14681 (2012).

- **It demonstrates high cytocompatability of 2-mercaptopropionic acid coated Ag_2S.**

17. Chen J, Feng L, Zhang M, Zhang X, Su H, Cui D. Synthesis of ribonuclease-A conjugated Ag2S quantum dots clusters via biomimetic route. *Mater. Lett.* 96 224-227 (2013).
18. Smith AM, Duan H, Mohs AM, Nie S. Bioconjugated quantum dots for in vivo molecular and cellular imaging. *Adv. Drug Deliv. Rev.* 60(11), 1226-1240 (2008).

19. Qi L, Gao X. Emerging application of quantum dots for drug delivery and therapy. *Expert Opin. Drug Deliv.* 5(3), 263-267 (2008).
20. Derfus AM, Chen AA, Min D-H, Ruoslahti E, Bhatia SN. Targeted quantum dot conjugates for siRNA delivery. *Bioconjugate Chem.* 18(5), 1391-1396 (2007).
21. Hocaoglu I, Demir F, Birer O *et al*. Emission tunable, cyto/hemocompatible, near-IR-emitting Ag 2 S quantum dots by aqueous decomposition of DMSA. *Nanoscale* 6(20), 11921-11931 (2014).
22. Yang H-Y, Zhao Y-W, Zhang Z-Y, Xiong H-M, Yu S-N. One-pot synthesis of water-dispersible Ag2S quantum dots with bright fluorescent emission in the second near-infrared window. *Nanotechnology* 24(5), 055706 (2013).
23. Duman FD, Khodadust R, Durmusoglu EG, Yagci MB, Acar HY. Impact of reaction variables and PEI/l-cysteine ratio on the optical properties and cytocompatibility of cationic Ag 2 S quantum dots as NIR bio-imaging probes. *RSC Adv.* 6(81), 77644-77654 (2016).
24. Zhao D, He Z, Chan W, Choi MM. Synthesis and characterization of high-quality water-soluble near-infrared-emitting CdTe/CdS quantum dots capped by N-acetyl-L-cysteine via hydrothermal method. *J. Phys. Chem. C* 113(4), 1293-1300 (2008).
25. Xue B, Deng D-W, Cao J *et al*. Synthesis of NAC capped near infrared-emitting CdTeS alloyed quantum dots and application for in vivo early tumor imaging. *Dalton Trans.* 41(16), 4935-4947 (2012).
26. Xiao L, Zhao D, Chan W-H, Choi MM, Li H-W. Inhibition of beta 1–40 amyloid fibrillation with N-acetyl-l-cysteine capped quantum dots. *Biomaterials* 31(1), 91-98 (2010).
27. Wang Q, Zhan G, Li C. Facile synthesis of N-acetyl-L-cysteine capped CdHgSe quantum dots and selective determination of hemoglobin. *Spectrochim. Acta A* 117 198-203 (2014).
28. Wang Q, Yu X, Zhan G, Li C. Fluorescent sensor for selective determination of copper ion based on N-acetyl-l-cysteine capped CdHgSe quantum dots. *Biosens. Bioelectron.* 54 311-316 (2014).
29. Yang T, He Q, Liu Y, Zhu C, Zhao D. Water-soluble N-Acetyl-L-cysteine-capped CdTe quantum dots application for Hg (II) detection. *J. Anal. Methods Chem.* 2013 (2013).
30. Heli H, Majdi S, Sattarahmady N. Ultrasensitive sensing of N-acetyl-l-cysteine using an electrocatalytic transducer of nanoparticles of iron (III) oxide core–cobalt hexacyanoferrate shell. *Sens. Actuators B Chem.* 145(1), 185-193 (2010).
31. Kelly GS. Clinical applications of N-acetylcysteine. *Altern. Med. Rev.* 3(2), 114-127 (1998).
32. Agarwal A, Said TM. Oxidative stress, DNA damage and apoptosis in male infertility: a clinical approach. *BJU Int.* 95(4), 503-507 (2005).
33. Kopke RD, Jackson RL, Coleman JK, Liu J, Bielefeld EC, Balough BJ. NAC for noise: from the bench top to the clinic. *Hear. Res.* 226(1-2), 114-125 (2007).
34. Feghali JG, Liu W, Van De Water TR. L-N-Acetyl-Cysteine protection against cisplatin-induced auditory neuronal and hair cell toxicity. L*aryngoscope* 111(7), 1147-1155 (2001).

•• **It demonstrates the protective effect of L-N-acetyl-cysteine against the side effects of chemotherepeutic drug cisplatin.**

35. Doroshow J, Locker GY, Ifrim I, Myers CE. Prevention of doxorubicin cardiac toxicity in the mouse by N-acetylcysteine. *J. Clin. Investig.* 68(4), 1053-1064 (1981).
36. Choi AO, Cho SJ, Desbarats J, Lovrić J, Maysinger D. Quantum dot-induced cell death involves Fas upregulation and lipid peroxidation in human neuroblastoma cells. *J. Nanobiotechnology* 5(1), 1 (2007).

•• **It discusses the mechanisms of quantum dot induced toxicity in human neuroblastoma cell line exposed to NAC-conjugated, NAC-capped and cysteamine-capped CdTe QDs.**

37. James LP, Mccullough SS, Lamps LW, Hinson JA. Effect of N-acetylcysteine on acetaminophen toxicity in mice: relationship to reactive nitrogen and cytokine formation. *J. Toxicol. Sci.* 75(2), 458-467 (2003).

38. Soenen SJ, Montenegro JM, Abdelmonem AM *et al*. The effect of nanoparticle degradation on poly(methacrylic acid)-coated quantum dot toxicity: The importance of particle functionality assessment in toxicology. *Acta Biomater.* 10(2), 732-741 (2014).
39. Morrell CN. Reactive oxygen species: finding the right balance. (2008).
40. Bazhin AV, Philippov PP, Karakhanova S. Reactive oxygen species in cancer biology and anticancer therapy. *Oxid. Med. Cell Longev.* 2016 (2016).
41. Jeong C-H, Joo SH. Downregulation of reactive oxygen species in apoptosis. *J. Cancer Prev.* 21(1), 13 (2016).
•• **It reports the decline of reactive oxygen species during apoptotic cell death.**
42. Cho S-G, Woo S-M, Ko S-G. Butein suppresses breast cancer growth by reducing a production of intracellular reactive oxygen species. *J. Exp. Clin. Cancer Res.* 33(1), 51 (2014).
•• **In this review it was indicated that N-acetyl-L-cysteine (NAC), a free radical scavenger, reduces ROS production and AKT phosphorylation, resulting in apoptotic cell death in breast cancer.**
43. Markoutsa E, Xu P. Redox potential-sensitive N-acetyl cysteine-prodrug nanoparticles inhibit the activation of microglia and improve neuronal survival. *Mol. Pharm.* 14(5), 1591-1600 (2017).
44. Xue C, Liu W, Wu J, Yang X, Xu H. Chemoprotective effect of N-acetylcysteine (NAC) on cellular oxidative damages and apoptosis induced by nano titanium dioxide under UVA irradiation. *Toxicol. In Vitro* 25(1), 110-116 (2011).
45. He Y-Y, Häder D-P. UV-B-induced formation of reactive oxygen species and oxidative damage of the cyanobacterium Anabaena sp.: protective effects of ascorbic acid and N-acetyl-L-cysteine. *J. Photochem. Photobiol. B* 66(2), 115-124 (2002).
46. Harada D, Anraku M, Fukuda H *et al*. Kinetic studies of covalent binding between N-acetyl-L-cysteine and human serum albumin through a mixed-disulfide using an N-methylpyridinium polymer-based column. *Drug Metab. Pharmacokinet.* 19(4), 297-302 (2004).
47. Giustarini D, Milzani A, Dalle-Donne I, Tsikas D, Rossi R. N-Acetylcysteine ethyl ester (NACET): a novel lipophilic cell-permeable cysteine derivative with an unusual pharmacokinetic feature and remarkable antioxidant potential. *Biochem. Pharmacol.* 84(11), 1522-1533 (2012).
48. Grinberg L, Fibach E, Amer J, Atlas D. N-acetylcysteine amide, a novel cell-permeating thiol, restores cellular glutathione and protects human red blood cells from oxidative stress. *Free Radic. Biol. Med.* 38(1), 136-145 (2005).
49. Wang B, Navath RS, Romero R, Kannan S, Kannan R. Anti-inflammatory and anti-oxidant activity of anionic dendrimer–N-acetyl cysteine conjugates in activated microglial cells. *Int. J. Pharm.* 377(1-2), 159-168 (2009).
50. Jiang P, Tian Z-Q, Zhu C-N, Zhang Z-L, Pang D-W. Emission-tunable near-infrared Ag2S quantum dots. *Chem. Mater.* 24(1), 3-5 (2011).
51. Madelung O. *Semiconductors:Data Handbook*. (3rd). (2004).
52. H.F.M. Marlene C. Morris EHE, Boris Paretzkin, Harry S. Parker, Nicolas C. Panagiotopoulos. *Standard X-ray Diffraction Powder Patterns*. Washington D.C. UNT Digital Library (1960).
53. Pavlin M, Bregar VB. Stability of nanoparticle suspensions in different biologically relevant media. *Dig. J. Nanomater. Bios.* 7(4), (2012).
54. Eruslanov E, Kusmartsev S. Identification of ROS using oxidized DCFDA and flow-cytometry. In: *Advanced protocols in oxidative stress II*, (Ed. Amstrong, Donald). Springer 57-72 (2010).
55. Nargi JL, Ratan RR, Griffin DE. p53-independent inhibition of proliferation and p21Waf1/Cip1-modulated induction of cell death by the antioxidants N-acetylcysteine and vitamin E. *Neoplasia* 1(6), 544-556 (1999).
56. Kawakami S, Kageyama Y, Fujii Y, Kihara K, Oshima H. Inhibitory effect of N-acetylcysteine on invasion and MMP-9 production of T24 human bladder cancer cells. *Anticancer Res.* 21(1A), 213-219 (2001).

57. Supabphol A, Muangman V, Chavasiri W, Supabphol R, Gritsanapan W. N-acetylcysteine inhibits proliferation, adhesion, migration and invasion of human bladder cancer cells. *J. Med. Assoc. Thai.* 92(9), 1171 (2009).
58. Lee Y-J, Lee DM, Lee C-H *et al*. Suppression of human prostate cancer PC-3 cell growth by N-acetylcysteine involves over-expression of Cyr61. *Toxicol. In Vitro* 25(1), 199-205 (2011).
59. Lee M-F, Chan C-Y, Hung H-C, Chou I-T, Yee AS, Huang C-Y. N-acetylcysteine (NAC) inhibits cell growth by mediating the EGFR/Akt/HMG box-containing protein 1 (HBP1) signaling pathway in invasive oral cancer. *Oral Oncol.* 49(2), 129-135 (2013).
60. Hann SS, Zheng F, Zhao S. Targeting 3-phosphoinositide-dependent protein kinase 1 by N-acetyl-cysteine through activation of peroxisome proliferators activated receptor alpha in human lung cancer cells, the role of p53 and p65. *J. Exp. Clin. Cancer Res.* 32(1), 43 (2013).
61. Ulukaya E, Ozdikicioglu F, Oral AY, Demirci M. The MTT assay yields a relatively lower result of growth inhibition than the ATP assay depending on the chemotherapeutic drugs tested. *Toxicol. In Vitro* 22(1), 232-239 (2008).

- **A detailed report illustrating the effect of N-acetyl cysteine and penicillamine on apoptosis.**

62. Amini A, Masoumi-Moghaddam S, Ehteda A, Morris DL. Bromelain and N-acetylcysteine inhibit proliferation and survival of gastrointestinal cancer cells in vitro: significance of combination therapy. *J. Exp. Clin. Cancer Res.* 33(1), 92 (2014).
63. Guan D, Xu Y, Yang M, Wang H, Wang X, Shen Z. N-acetyl cysteine and penicillamine induce apoptosis via the ER stress response-signaling pathway. *Mol. Carcinog.* 49(1), 68-74 (2010).
64. Tsai J-C, Jain M, Hsieh C-M *et al*. Induction of apoptosis by pyrrolidinedithiocarbamate and N-acetylcysteine in vascular smooth muscle cells. *J. Biol. Chem.* 271(7), 3667-3670 (1996).
65. Liu M, Pelling JC, Ju J, Chu E, Brash DE. Antioxidant action via p53-mediated apoptosis. *Cancer Res.* 58(8), 1723-1729 (1998).
66. Havre PA, O'reilly S, Mccormick JJ, Brash DE. Transformed and tumor-derived human cells exhibit preferential sensitivity to the thiol antioxidants, N-acetyl cysteine and penicillamine. *Cancer Res.* 62(5), 1443-1449 (2002).
67. Navath RS, Kurtoglu YE, Wang B, Kannan S, Romero R, Kannan RM. Dendrimer− drug conjugates for tailored intracellular drug release based on glutathione levels. *Bioconjugate Chem.* 19(12), 2446-2455 (2008).
68. Lepri E, Gambelunghe C, Fioravanti A, Pedini M, Micheletti A, Rufini S. N-acetylcysteine increases apoptosis induced by H2O2 and mo-antiFas triggering in a 3DO hybridoma cell line. *Cell Biochem. Funct.* 18(3), 201-208 (2000).
69. Rieber M, Rieber MS. N-Acetylcysteine enhances UV-mediated caspase-3 activation, fragmentation of E2F-4, and apoptosis in human C8161 melanoma: inhibition by ectopic Bcl-2 expression. *Biochem. Pharmacol.* 65(10), 1593-1601 (2003).
70. Deshpande V, Kehrer JP. Mechanisms of N-acetylcysteine-driven enhancement of MK886-induced apoptosis. *Cell Biol. Toxicol.* 22(4), 303-311 (2006).
71. Zhang L, Cheng X, Gao Y *et al*. Induction of ROS-independent DNA damage by curcumin leads to G2/M cell cycle arrest and apoptosis in human papillary thyroid carcinoma BCPAP cells. *Food Funct.* 7(1), 315-325 (2016).
72. Yamashita N, Kawanishi S. Distinct mechanisms of DNA damage in apoptosis induced by quercetin and luteolin. *Free Radic. Res.* 33(5), 623-633 (2000).

- **In this study it was shown that ROS is not required for DNA damage.**

73. Santus P, Corsico A, Solidoro P, Braido F, Di Marco F, Scichilone N. Oxidative Stress and Respiratory System: Pharmacological and Clinical Reappraisal of N-Acetylcysteine. *COPD* 11(6), 705-717 (2014).

74. Dekhuijzen PNR. Antioxidant properties of N-acetylcysteine: their relevance in relation to chronic obstructive pulmonary disease. *Eur. Respir. J.* 23(4), 629-636 (2004).
75. Vanzandwijk N. N-Acetylcysteine for Lung-Cancer Prevention. *Chest* 107(5), 1437-1441 (1995).

Supplementary Information

Development of NIR luminescent N-acetyl-L-cysteine coated Ag_2S quantum dots with differential therapeutic effect

Characterization methods

The absorbance spectra of the quantum dots were recorded using a Shimadzu UV-Vis-NIR spectrometer in the 500–1100 nm range. Photoluminescence spectra in the near-infrared region were recorded using a homemade set up : a 1/8 Newport Cornerstone 130 monochromator equipped with a 600 L mm^{-1} grating which works in the 400–1100 nm scale, a femtowatt sensitive Si detector (Thorlabs PDF10A, 1.4 x 10^{-15} W $Hz^{-1/2}$) and a frequency doubled output of a DPSS laser (532 nm). Measurements were performed with 0.5 mm slit width and a 590 nm long pass filter. Brus equation (Eq. 1) was used to calculate the crystal sizes of Ag_2S nanoparticles from the absorption edge found from the absorption spectra of QDs [49, 50].

$$\Delta E = \frac{\hbar^2\pi^2}{8R^2}\left[\frac{1}{m_e} + \frac{1}{m_h}\right] - 1.8\,\frac{e^2}{\varepsilon_{Ag_2S} 4\pi\varepsilon_0 R} \qquad \text{(Eq. 1)}$$

In Eq. 1, R is the radius of the Ag_2S, m_e (=0.286 m_0)is effective electron mass and m_h (=1.096)is hole mass of inorganic core, ε_{Ag_2S} (5.95) is the dielectric constant and ΔE is the band gap energy difference between the nanocrystal and the bulk Ag_2S[51].

Quantum yield (QY) of the QDs was calculated based on the procedures in the literature using LDS 798 NIR dye (QY 14% in methanol, reported by the producer) as a reference [21, 23]. Five different concentrations of the dye were prepared in methanol and aqueous NAC-Ag_2S QDs

with absorption below 0.10 at the excitation wavelength (532 nm) were prepared. The PL spectra of all concentrations were recorded and integrated areas under the emission peaks were plotted against the concentrations. QY was calculated from the ratio between the slope of the sample (m_{QD}) and the slope of the dye ($m_{standard}$) using the refractive index (η) of water and methanol as follows:

$$QY_{QD} = \left(\frac{m_{QD}}{m_{standard}}\right)\left(\frac{\eta_{water}^{2}}{\eta_{methanol}^{2}}\right) \times 100 \qquad \text{(Eq. 2)}$$

Fluorescence lifetime analysis was performed using a Horiba Fluorolog equipped with TCSPC Triple Illuminator. 456 nm Horiba Nanoled pulsed diode light source (pulse duration 1.2 ns) was employed. Measurement time of 400 ns was taken for 4096 channel to obtain high-resolution measurements.

Hydrodynamic size and zeta potential of the aqueous nanoparticles were measured using a Malvern Zetasizer Nano-ZS. Organic elemental analysis was performed by a Thermo Scientific Flash 2000 Organic Elemental Analyzer. 2-3 mg dried sample and vanadium pentoxide which is a typical oxygen donor that allows the total conversion of sulphur, were placed into a tin capsule and loaded to the combustion reactor via the Thermo Scientific MAS 200R autosampler. To calculate the organic elemental content of the sample, a standard curve drawn by 2,5-bis-(5-tert-butyl-2-benzoxazol-2-yl) thiophene (BBOT) was used.

Particle shapes and morphologies were determined by a transmission electron microscopy (TEM Philips-FEI-Tecnai G2 F30) operating at an accelerating voltage of 200 kV. Fourier transform infrared (FTIR) spectra of the QDs were taken on a Thermo Scientific Nicolet iS10 FT-IR 4000-650 cm^{-1}, single reflection diamond ATR spectrometer. Ag^{+} content in QDs was measured

using an Agilent 7700×ICP-MS (inductively coupled plasma–mass spectroscopy). NAC-Ag_2S QDs were digested with 1 mL of acid mixture including suprapur sulphuric acid and suprapur nitric acid (1:9, v/v), and then diluted to 10 ml with DI water in a volumetric flask for the ICP measurements.

Table S1.

Organic elemental analysis of NAC-Ag_2S QDs measured by Organic Elemental Analyzer

Element	**Weight %**
Nitrogen	3.3
Carbon	20.2
Hydrogen	2.4
Sulphur	10.7
Totals	36.6

Table S2.

Equivalent concentrations of free NAC to NAC-Ag_2S QDs.

NAC (μg/mL)	0.037	0.073	0.14	0.29	0.57	1.15	2.29	4.58	9.15	18.3	36.6	73.2
NAC-Ag_2S (μg/mL)	0.10	0.20	0.39	0.78	1.56	3.13	6.25	12.5	25	50	100	200

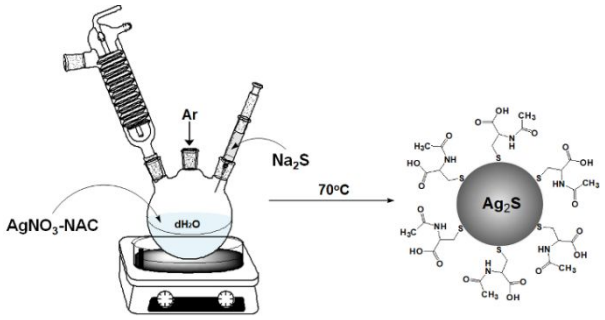

Fig. S1. Aqueous synthesis of NAC-Ag_2S QDs.

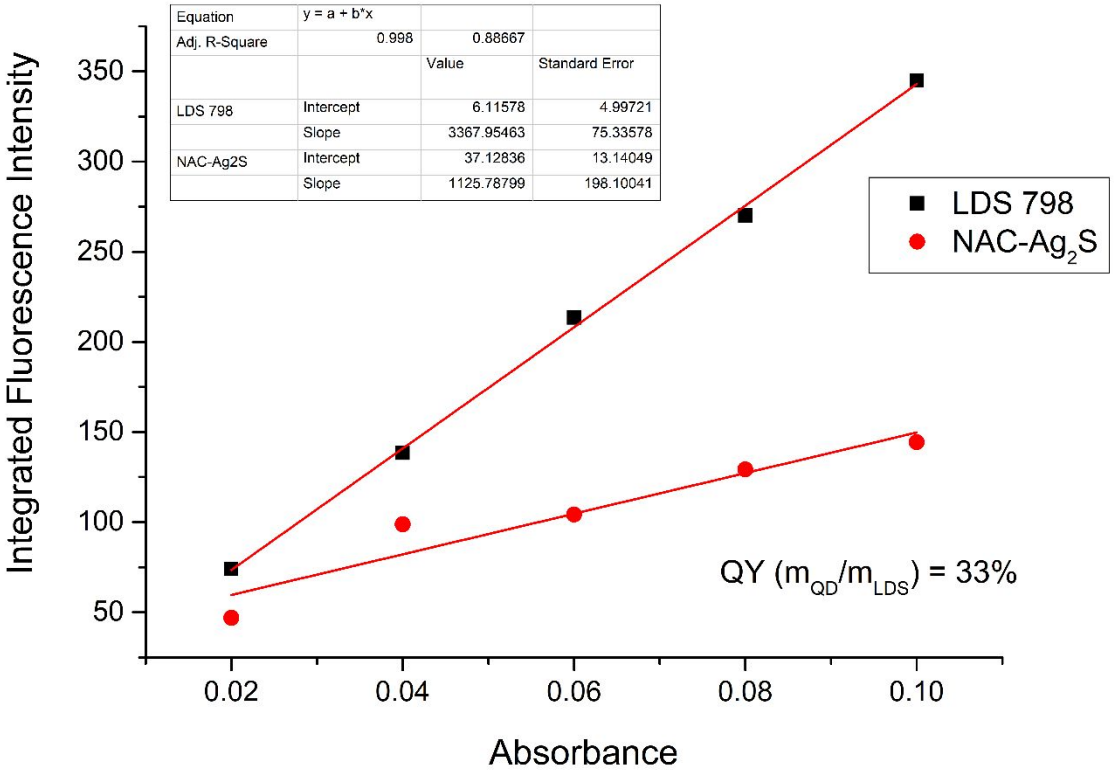

Fig. S2. Plot of the integrated luminescence intensities of the reference dye, LDS 798, and NAC-Ag_2S QDs against the absorbance intensities. Inset shows the slope of each line corresponding to the dye and NAC-Ag_2S.

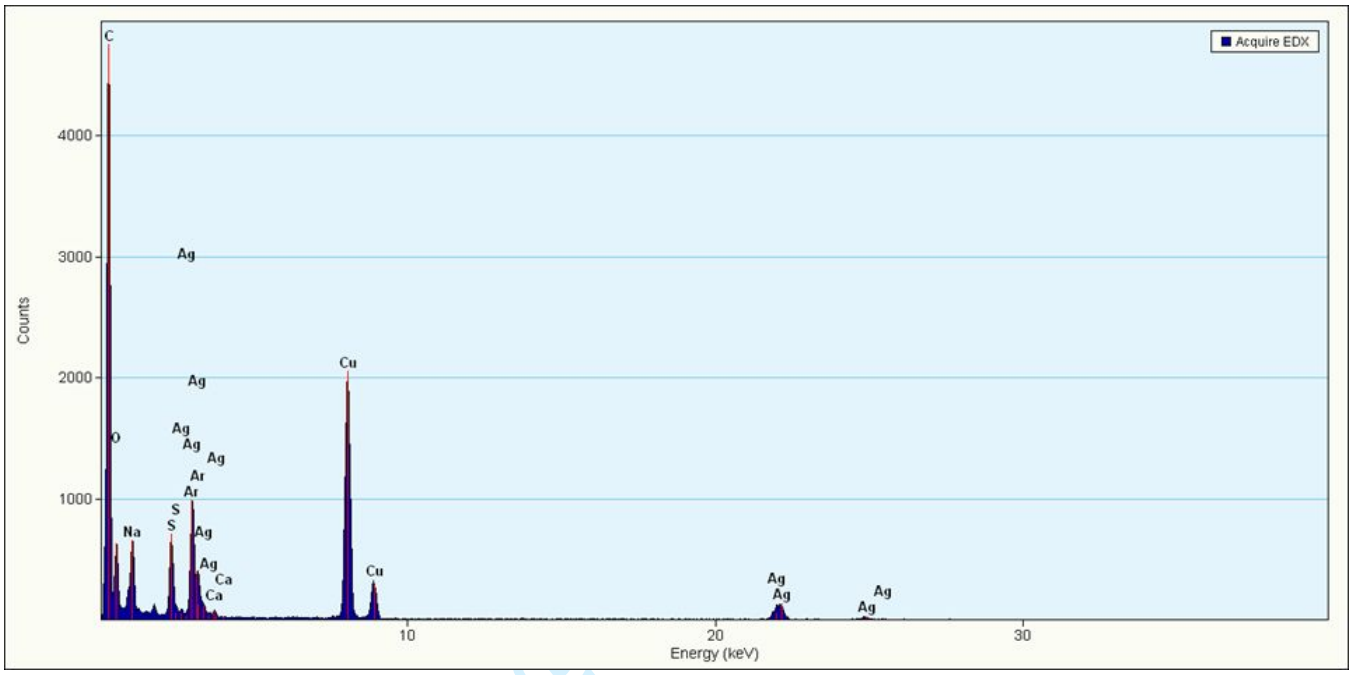

Fig. S3. EDX analyses of NAC-Ag_2S QDs (QD3).

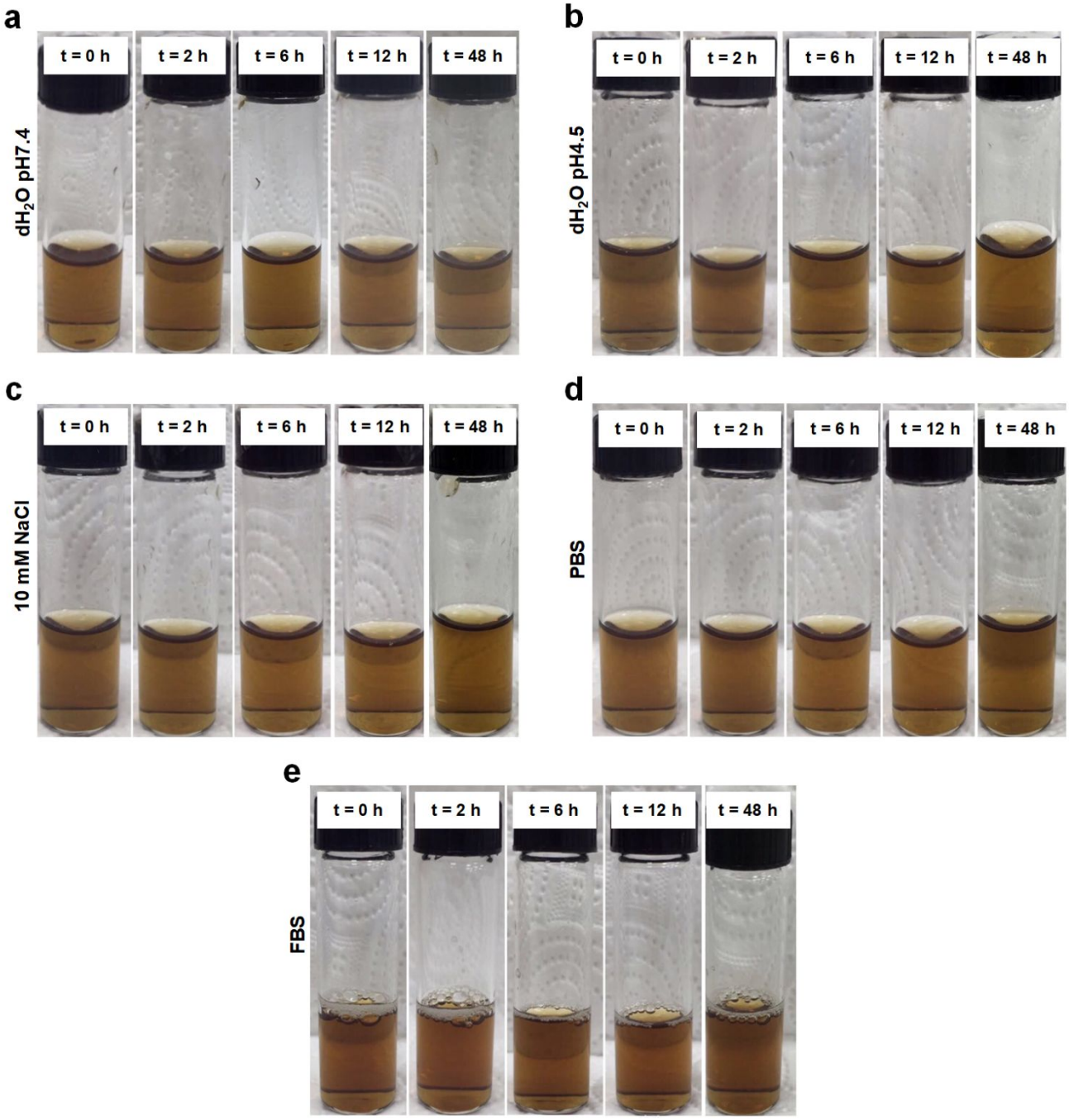

Fig. S4. Time dependent colloidal stability of NAC-Ag_2S QDs in different media. (a) in dH_2O, pH7.4; (b) in dH_2O, pH4.5; (c) in 10 mM NaCl; (d) in PBS; (e) in FBS.

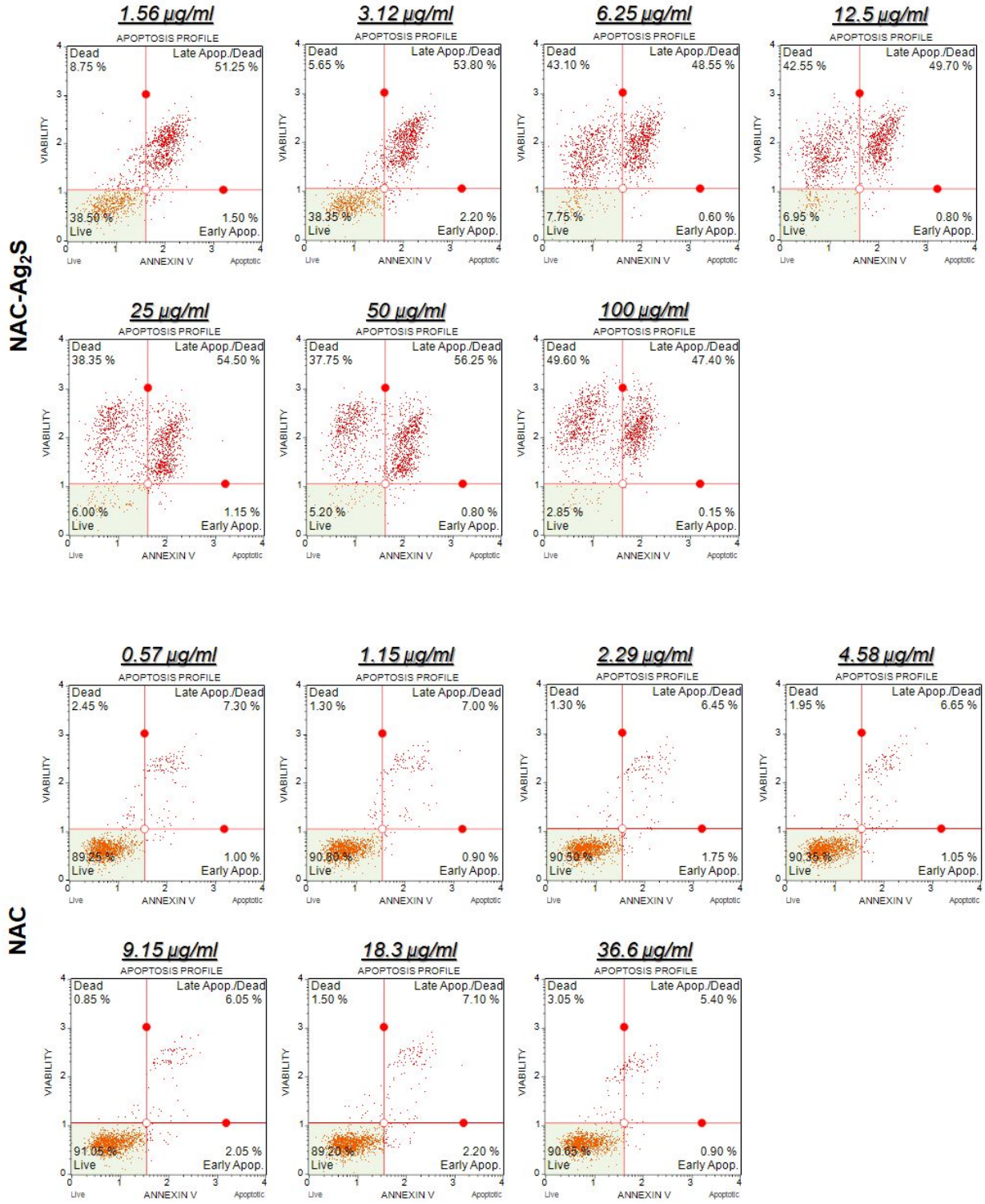

Fig. S5. Determination of apoptosis in MCF-7 cells treated with NAC-Ag_2S QDs or free NAC for 48 h and assessed by Annexin V/Dead Cell assay using flow cytometry. Percentages of cells were presented in each quadrant.

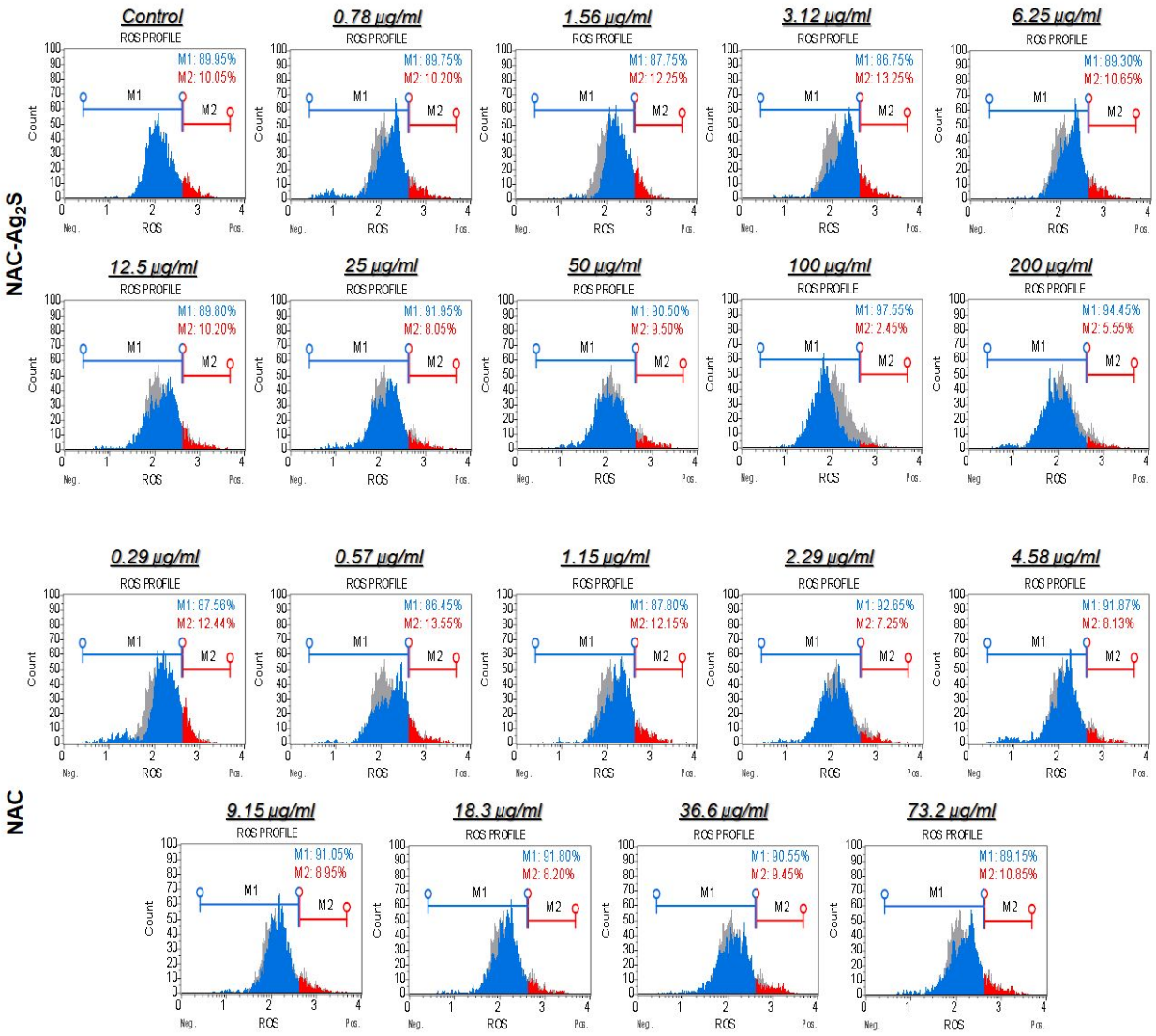

Fig. S6. Intracellular ROS level of MCF-7 cells treated with NAC-Ag_2S QDs or equivalent free NAC, measured by ROS kit and flow cytometer 48 h after the exposure. Data represents mean ± SD of three experiments ($p < 0.05$(*), $p < 0.01$ (**)).

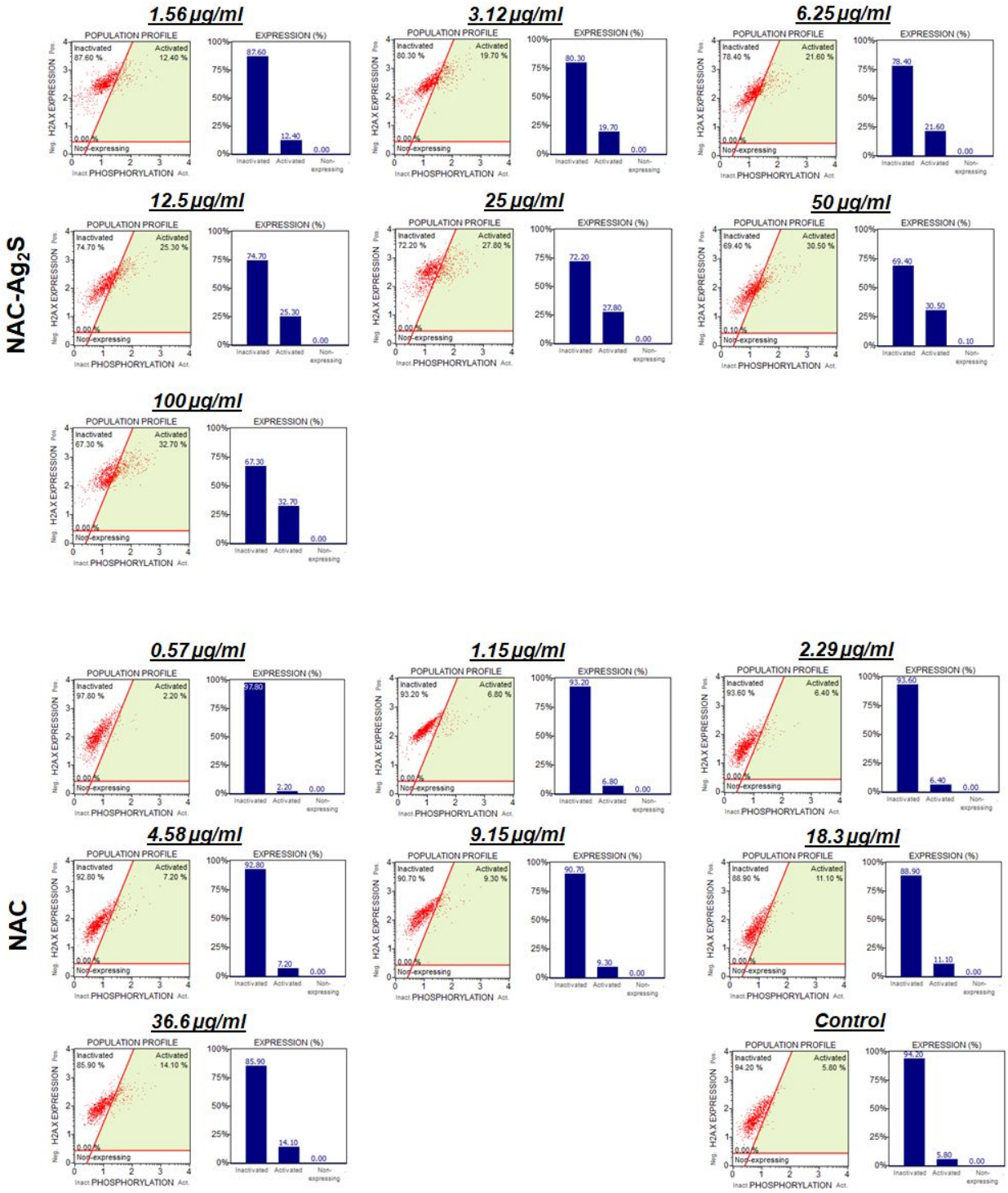

Fig. S7. γH2A.X levels in MCF-7 cells treated with NAC-Ag_2S QDs and NAC measured by flow cytometry 48 h after treatment.